CHARLES UNIVERSITY IN PRAGUE
FACULTY OF MATHEMATICS AND PHYSICS

MASTER THESIS

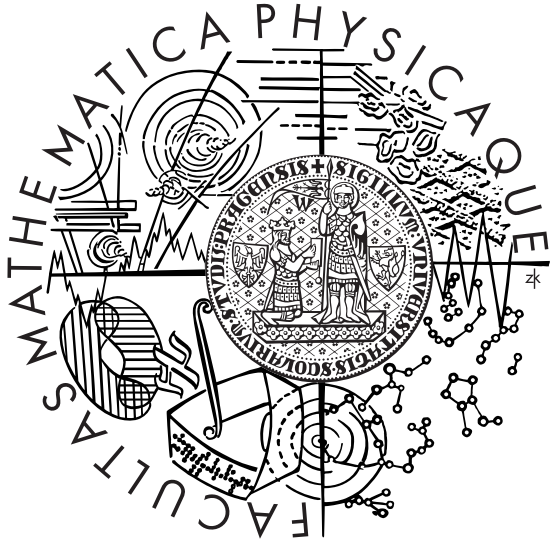

Determination of the Mass Distribution in the Galactic Centre from the Stellar Motions

Jaroslava Schovancová

Astronomical Institute, Charles University in Prague
Supervisor: RNDr. Ladislav Šubr, Ph.D.
Study Programme: Physics
Study Plan: Astronomy and Astrophysics

Ráda bych na tomto místě co nejsrdečněji poděkovala všem, kteří mi poskytli podporu při tvorbě této práce. Vedoucímu diplomové práce Dr. Ladislavu Šubrovi děkuji za cenné připomínky a rady v průběhu práce. Ivaně Stoklasové děkuji za pečlivé přečtení celého textu a užitečné komentáře. Kolegům Ivaně Ebrové, Miroslavu Křížkovi a Tomáši Pecháčkovi děkuji za dobré rady a kolegialní podporu v závěrečné fázi práce.

Ráda bych poděkovala všem, kteří mi umožnili strávit nádhernch deset měsíců studia v Bonnu na Argelander Institut für Astronomie. Díky patří zejména garantům Erasmus smlouvy, Dr. Ladislavu Šubrovi a Prof. Dr. Ulrichu Kleinovi, fakultní koordinátorce programu Erasmus Dr. Věře Hrachové a pracovníkům Evropské kanceláře Univerzity Karlovy v Praze. Vřelé díky patří Prof. Dr. Pavlu Kroupovi a členům jeho pracovní skupiny za velice přátelské a motivující prostředí.

Děkuji za možnost počítání své diplomové práce na clusterech Astronomického stavu Univerzity Karlovy v Praze. Ráda bych poděkovala Dr. Jiřímu Chudobovi za možnost počítání na gridové infrastruktuře projektu EGEE-II.

V neposlední řadě si poděkování zaslouží moje rodina za podporu poskytovanou během celé doby mého studia.

Prohlašuji, že jsem svou diplomovou práci napsala samostatně a výhradně s použitím citovaných pramenů. Souhlasím se zapůjčováním práce.

V Praze dne 10. srpna 2007 Jaroslava Schovancová

Contents

Název práce: Určování rozložení hmoty v jádře Galaxie z pohybů hvězd
Autor: Jaroslava Schovancová
Katedra (ústav): Astronomický ústav Univerzity Karlovy v Praze
Vedoucí diplomové práce: RNDr. Ladislav Šubr, Ph.D.
E-mail vedoucího: subr@sirrah.troja.mff.cuni.cz
Abstrakt: Nedávná infračervená pozorování Galaktického jádra nasvědčují tomu, že se v blízkosti supermasivní černé díry Sgr A⋆ nachází nejméně jedna koherentně rotující struktura mladých hvězd a kulová hvězdokupa složená ze starých hvězd. Radioastronomická pozorování oblasti Galaktického jádra zároveň ukazují na přítomnost několika struktur mezihvězdné hmoty, z nichž nás zajímal především nejhmotnější útvar, molekulární disk (tzv. circum-nuclear disk). Pozorování ukazují, že korotující mladý hvězdný disk je téměř kolmý na uvažovaný molekulární disk. Modelovali jsme pohyb testovacích částic představujících hvězdy korotujícího hvězdného disku v dominantním potenciálu Sgr A⋆ porušeném axiálně symetrickou a sférickou poruchou a hledali jsme množinu parametrů popisujících studovaný model Galaktického centra konzistentní s pozorováními jednotlivých zdrojů potenciálu, ale především s pozorováními korotujícího hvězdného disku. Předpokládali jsme, ze mladý hvězdný disk existuje jako stabilní struktura po dobu 6 miliónů let. Zjistili jsme, že hmotnost molekulárního disku odpovídající 0,2 až 0,4 hmotnosti Sgr A⋆ je v souladu se současnými pozorováními korotujícího hvězdného disku a že tento hvězdný disk s velkou pravděpodobností v době svého vzniku byl téměř kolmý k molekulárnímu disku a zároveň nebyl geometricky rozevřený více nežli 2 °.
Klíčová slova: galaxie: jádra — Galaxie: centrum — mladé hvězdy: dynamika

Title: Determination of the Mass Distribution in the Galactic Centre from the Stellar Motions
Author: Jaroslava Schovancová
Department: Astronomical Institute, Charles University in Prague
Supervisor: RNDr. Ladislav Šubr, Ph.D.
Supervisor's e-mail address: subr@sirrah.troja.mff.cuni.cz
Abstract: Recent NIR observations of the Galactic Centre suggest existence of two young stellar structures with a coherent rotation pattern in vicinity of the super-massive black hole Sgr A⋆ and a spherical cluster of old stars. At the same time, radioastronomical observations of the Galactic Centre show that there are several ISM structures in that region. We focused our interest on the heaviest of the observed ISM structures, on a molecular disk (circum-nuclear disk, CND) and its gravitational interaction with the young stellar disk. The observations show that the stellar disk is almost perpendicular to the CND. We have modelled the clockwise stellar disk as a set of test particles influenced by a dominating Keplerian potential of Sgr A⋆ perturbed by an axi-symmetric and a spherical perturbation and we have explored the parameter space describing the Galactic Centre model consistent with observations of the stellar disk. We assumed that the young stellar disk is a stable structure for 6 Myr. We have found that the mass of the CND corresponding to 0.2 to 0.4 mass of the Sgr A⋆ is consistent with recent NIR observations of the young stellar disk and that this stellar disk was almost perpendicular to the CND and very well defined planar structure with a characteristic initial opening angle of the stellar disk that did not exceed 2 °.
Keywords: galaxies: nuclei — Galaxy: centre — young stars: dynamics

List of Figures

List of Abbreviations

AGB 4
Asymptotic giant branch

CCWS 4
Counter-clockwise stellar disk

CND 6
Circum-nuclear disk

CWS 4
Clockwise stellar disk

GC 3
Galactic Centre

IR 3
Infra-red

NIR 4
Near-infrared

SMBH 3
Super-massive black hole

Preface

A galactic nucleus represent a complex system which harbours a central compact object, interstellar medium and a dense stellar cluster. Individual components of the system mutually interact and we witness the most powerful processes in the Universe. Super-massive black holes, which reside in the most of galactic nuclei have the mass of about $10^6 - 10^9\,M_\odot$. Active galactic nuclei radiate with luminosities of the order of $10^{49} - 10^{51}$ W, which is by 23 to 25 orders of magnitude more powerful than our nearest star. Stellar densities in the nuclei of galaxies are $\approx 10^9$ higher than in the solar neighbourhood. Hence, galactic nuclei represent unique laboratories for exploration of dynamics in a very dense and complex environment. Luckily, there is an option to explore the Galactic centre in more detail due to its proximity. The Centre of Galaxy is rather quiet compared to an AGN, but still eventful compared to our neighbourhood.

The Galactic Centre is situated in the southern hemisphere of the sky in the constellation of Sagittarius. Observations of the velocity dispersion of gas around the dynamical centre of the Galaxy show that there is a very compact object in that region. There was no proven evidence what kind of compact object it could be twenty years ago. Since then, improvements of the observational technique have enabled to resolve smaller and smaller stellar clusters as far as today diffraction limited observations with 8 m and 10 m class telescopes resolve single stars. Measurements of proper stellar motions resulted in a more accurate mass estimate of the central object. Mass of $\simeq 3/5 \times 10^6\,M_\odot$ and a diameter much less than 1 AU suggest that this central object is a super-massive black hole.

Detailed exploration of the surroundings of the central object gave rose to several interesting puzzles. The most crucial one for this Thesis is the presence of several tens of young stars in couple of groups in the Galactic Centre. There are couple of B-type stars, known as S-stars, on very eccentric orbits in the central arcsecond of the region. Another group of O- and B-type stars is a bit further from the central super-massive black hole, between 1″ and 12″ (0.04 pc and 0.48 pc), where resides at least one structure

of young stars with a coherent rotation pattern. This stellar cluster offers us an interesting question: how such a young stellar structure can form? Since the stars are several Myr young, they are a result of a recent star formation in the Galactic centre. Observations show that the young stellar cluster with a corotating pattern, with respect to the Galaxy rotation, is a disk-like structure with an opening angle of $\approx 14^\circ$ and the stars have intermediate eccentrities. However, such a stellar disk was observed also in the Andromeda galaxy.

There are two scenarios of the formation of the young stellar disk. The first one suggests that the formation of young stars arose via a fragmentation of an accretion disk. The other one proposes that the stellar disk formed after infall of a stellar cluster coming from the outer parts of the Galactic Centre.

However, the groups of young stars are not the only stars in vicinity of the super-massive black hole. Near-infrared observations show that there is a stellar cusp with the total mass similar to that of the central black hole within a few pc and a broken power-law profile of the mass-density.

Radioastronomical observations of the Galactic Centre region show the distribution and velocity dispersion of several structures of the interstellar medium. The heaviest structure within the central 2 pc is a clumpy molecular ring, known as the circum-nuclear disk. Observers estimate the mass of this molecular ring as $\approx 1/3\, M_\bullet$.

The gravitational interaction between the young stars forming a stellar disk and the other constituents of the Galactic centre is a subject of interest of this Thesis. We consider a simplified model of the Galactic centre, which describes the gravitational potential of that region. In this model we investigate the dynamics of the young stellar disk. The aim of our effort is to find a set of parameters describing the Galactic Centre environment, which correspond to both near-infrared and radioastronomical measurements and are in agreement with the observations of the young stellar cluster. Such a toy-model of the Galactic Centre helps us to better understand the stellar formation in vicinity of the central super-massive black hole.

A basic overview of the observations of the Galactic Centre region in Chapter 1. The model of the Galactic Centre and the results are described in Chapter 2. Consequences of the acquired results are discussed in Chapter 3.

1 The Central Two Parsecs Over The Past Three Decades

This chapter should familiarise the reader with the results of the past three decades of the Galactic Centre observations with emphasis on the objects important for this work. However, we do not intend to give the overall current state-of-art review.

1.1 Where is the Galactic Centre?

The innermost part of our Galaxy is situated on the southern celestial hemisphere in the direction of the constellation of Sagittarius. In this work the Galactic Centre (GC) represents the region with the radius 2 pc of the dynamical centre of the Galaxy. The current GC observations show that there is a super-massive black hole (SMBH) located at the dynamical centre of our Galaxy. This SMBHs environment can be observed in radio and infra-red (IR) wavelengths.

The first determination of the distance from the Sun to the dynamical centre of the Galaxy, R_0, published by Shapley, 1918 based on the Cepheid magnitude-period relation was estimated as $R_0 \approx 13$ kpc. According to the review by Reid, 1993, the best estimate results from H_2O maser proper motions: $R_0 = (8.0 \pm 0.5)$ kpc.

The most recent value of $R_0 = (7.62 \pm 0.32)$ kpc by Eisenhauer et al., 2005. This estimate was obtained by solving the Keplerian orbits (the corresponding central mass estimate is $M_\bullet = (3.61 \pm 0.32) \times 10^6 M_\odot$) of the innermost individual stars from the radial velocity and proper-motions measurements.

1.2 What is Sgr A* ?

The compact radio-source nowadays referred to as the Sgr A* was first observed by Becklin & Neugebauer, 1968. Since those times there were several ideas what kind of an astrophysical object the Sgr A* should be

according to the current mass-density estimates determined from IR observations: from a very dense cluster, through a fermion ball, a cluster of neutron stars, white dwarfs and stellar black holes – see Fig. 12 in Schödel et al., 2003. These central object hypotheses were rejected, because the observations of the central object show $10 - 10^{15}\times$ lower mass-densities than deduced from stellar motions and they would not be luminous enough either. The recent observations resulted in agreement that Sgr A* is a supermassive black hole SMBH. The radio-source radiates then due to the accretion of interstellar material onto the SMBH. The celestial position of Sgr A* is RA=$17^h45^m40.0409^s$ and DE=-29°00′ 28.118″ (J2000.0), see Reid & Brunthaler, 2004.

1.3 Stellar populations in the Galactic Centre

The SMBH in the centre of our Galaxy is surrounded by a nuclear stellar cluster, gas and dust. The Galactic Centre (GC) region is mostly observed in near-infrared (NIR) wavelengths, the most often used bands are K-band (2.2 μm), L-band (3.5 μm) and H-band (1.65 μm).

The central pc contains different stellar populations. Genzel et al., 2003 summarise that the radial distribution of stars follows a power-law distribution with the power-law index $\alpha \sim 1.3 - 1.4$. The stellar population in the GC can distinct three groups of stars: galactic bulge-like, a cusp within 1.5″ and the innermost cusp.

The outer part of the central pc contains the same stellar population as the galactic bulge: synthesis of an old, metal rich stellar population, contributed by young, early- and late-type stars. The central pc is dominated by old (1-10 Gyr) red giants with K $\geq$ 13 mag.

There are $\sim$ 12 luminous blue super-giants ($K \sim 9 - 12$ mag) which suggest the recent star formation (age of 2-7 Myr). The next stellar component are bright asymptotic giant branch (AGB) stars with intermediate-mass and intermediate-age $\geq$ 100 Myr, $K \sim 10 - 12$ mag. The next component of the central pc are dust-embedded stars associated with gaseous mini-spiral.

The hot topic of the GC region research are the young stars in the inner 0.15 pc. In the innermost part of the GC, in the central 0.01 pc, there is a group of young stars known as the S-stars. Most of the massive early-type stars in the distance of 0.05-0.15 pc two disk-like structures were formed, referred to as clockwise (CWS) and counter-clockwise (CCWS) disks.

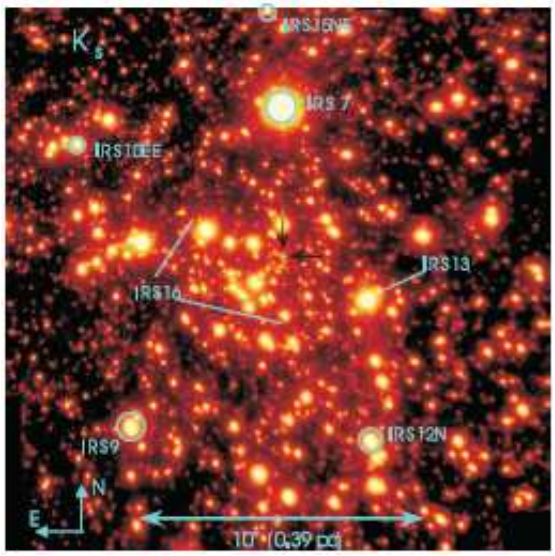

Figure 1.1: The central 20″ in NIR band K_S (2.2 μm) from Genzel et al., 2003. The black arrows point to the position of Sgr A* .

1.3.1 Spherical cluster

The spherical cluster is dominated by (1-10) Gyr old red giants. Genzel et al., 2003 analysed NIR images of the central region taken before 2002 by ESO NTT and Keck telescopes and new images taken at ESO VLT. They counted sources in these images in anulli and corrected the number counts for incompleteness. They found that the density profile of the spherical cluster of old stars has a broken power-law mass density. The central parsec in NIR is shown in Fig. 1.1. Schödel et al., 2007 extended measurements of the central region. They estimated the break radius to be

$$\rho(r) \propto r^{-\alpha},\ R_{\rm br} = (6 \pm 1)\,'' \tag{1.1}$$

and the cusp profile reads

$$\alpha = \begin{cases} 1.19 \pm 0.05 & r \leq R_{\rm br}, \\ 1.75 \pm 0.05 & r > R_{\rm br}. \end{cases} \tag{1.2}$$

The cusp with $\alpha = 1.75$ corresponds to a theoretical estimate for a relaxed single-mass stellar population by Bahcall & Wolf, 1976.

1.3.2 Young stellar disk

Genzel et al., 2003 reported the presence of at least one structure of young massive O- and B-type stars (Genzel et al., 2003, Ghez et al., 2005) with a coherent rotation pattern within 0.4 pc. They found a well defined clockwise stellar disk with a sharp inner margin (0.04 pc) and a worse defined counter-clockwise disk. Genzel et al., 2003 (normalised and projected angular momentum in the direction of the line-of-sight), Levin & Beloborodov, 2003, Beloborodov et al., 2006 (fit of velocity vectors of stars and χ^2 test of planarity of such a structure) and Paumard et al., 2006 (velocities of a planar structure expressed in spherical coordinates show a cosine pattern in a grid of $(\phi;\ \text{cotan}\,\theta)$) proposed several analyses to confirm that the observed structure is disk-like. Beloborodov et al., 2006 and Paumard et al., 2006 suggest that the clockwise disk thickness is $\langle |h|/R \rangle = 0.12 \pm 0.03\ (14^\circ \pm 4^\circ)$ and that this stellar disk is almost perpendicular to the circum-nuclear molecular disk.

These structures became an interesting puzzle in the GC research, because their age (6 ± 2) Myr suggests that these young stars are result of a recent star formation in GC. There are two scenarios of the formation of the young stellar disk. The first one suggests that the stellar disk formed via fragmentation of a accretion disk (Collin & Zahn, 1999, Levin & Beloborodov, 2003, Goodman, 2003). The other one proposes infall of a young stellar cluster into the central region (McMillan & Portegies Zwart, 2003, Gürkan & Rasio, 2005, Freitag et al., 2006).

The young stars have intermediate eccentrities $e \lesssim 0.35$ (Paumard et al., 2006). Alexander et al., 2007 suggest that such eccentrities are attainable from initially circular orbits within 6 Myr, assuming the top-heavy IMF, due to two-body interactions.

1.4 Circum-nuclear disk

Radioastronomical measurements of the velocity dispersion of gas in the Galactic Centre revealed that there are several ISM structures. The heaviest one, first detected by Becklin et al., 1982 as double-lobed emission at 50 and 100 μm, is a clumpy molecular ring with a well defined inner radius $\sim$ 1.5 pc with the thickness of $\sim$ 0.4 pc at the inner edge and the outer edge at $3 - 4$ pc with the thickness up to 2 pc. The circum-nuclear disk (CND) consists of neutral and ionised gas. The current estimate of the mass of the CND is $M_{\text{CND}} = 10^6\, M_\odot$ (Christopher et al., 2005). We overview the mass estimates in Table 1.1.

Table 1.1: Measurements of $M_{\rm CND}$ from the gas emission.

Neutral gas			
Year	Mass $[M_\odot]$	Emission	Paper
1981	10^3	[OI]	Lester et al., 1981
1984	2×10^3	[OI]	Genzel et al., 1984
1985	10^4	CO	Harris et al., 1985
1985	2×10^3	—	Genzel et al., 1985, review
1985	10^5	NH_3, HNCO, CO	Armstrong & Barrett, 1985
1986	10^3	HI & molecules	Hyland, 1984
1993	3×10^3	HI	Yusef-Zadeh et al., 1993
1993	10^4	molecular, atomic	Jackson et al., 1993
1995	10^5	CO⇒HI	Zhao et al., 1995
1996	10^4	—	Mezger et al., 1996, review
Ionized gas			
Year	Mass $[M_\odot]$	Emission	Paper
1985	3×10^5	HII	Ho et al., 1985
1993	2×10^6	HII	Gray et al., 1993
1999	10^4	H_α	Anantharamaiah et al., 1999
Neutral and Ionized gas			
Year	Mass $[M_\odot]$	Emission	Paper
1987	10^4	—	Genzel et al., 1987, review
2001	10^4	CO, H_2, HCN, CII, [OI]	Vollmer et al., 2001, review
2004	3×10^5	HCO^+, H_α	Shukla et al., 2004
2005	10^6	HCN, HCO^+	Christopher et al., 2005

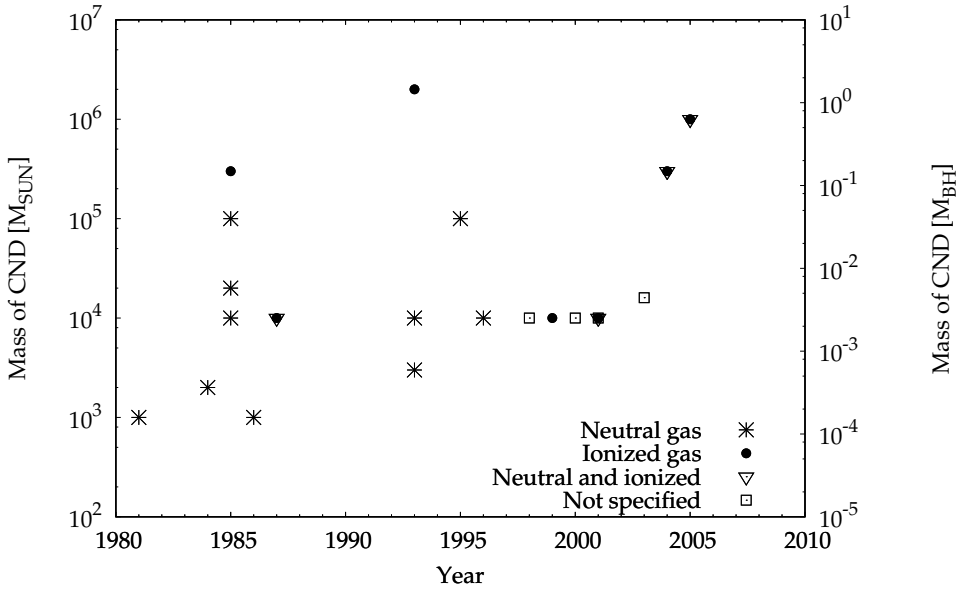

2 Model

The main aim of this thesis is to find parameters describing the Galactic Centre model such that the simulated motion of the clockwise stellar disk is consistent with the NIR observations. The stellar disk is modelled as a set of test particles moving under the influence of the gravitational potential dominated by the central potential of the super-massive black hole. This central Keplerian potential is perturbed by an axi-symmetrical potential due to the CND and by a spherical potential due to the cluster of old stars. The perturbing potential causes a secular evolution of the orbital elements of the test particles. This long-term evolution leads to a deformation of the initial spatial structure. The parameters of the perturbing potential and the initial orbital elements of the test particle determine the rate of secular evolution of the orbital elements. Hence, scanning the parameter space of the modelled CWS disk system enables us to set limits on some of the parameters of the potential, e.g. limit the mass of the CND in a way independent of the observed molecular emission.

2.1 Model of the Galactic Centre

Our model of the Galactic Centre region is described by the gravitational potential

$$\Phi_{\mathrm{per}} = \Phi_{\bullet} + \Phi_{\mathrm{sphe}} + \Phi_{\mathrm{CND}}. \tag{2.1}$$

This potential describes the gravitational influence of a SMBH ($\Phi_{\bullet}$), a molecular ring (Φ_{CND}), and a spherical cusp of old stars (Φ_{sphe}) on a young stellar disk. We consider all the contributing potentials as completely Newtonian. We do not consider any kind of non-gravitational interactions in our model.

Taking into account symmetries of the Galactic Centre model (2.1), we define a coordinate system in which we perform our numerical simulations. Let the SMBH be in the origin of the coordinate system. The axial symmetry of the CND potential enables us to define the equatorial plane ($Z = 0$) such that the axi-symmetrical perturbation CND resides in the equatorial plane, i.e. $Z_{\mathrm{CND}} \equiv 0$. The normal vector to the CND is then parallel to the Z axis. Orbital elements Ω, i and ω are then defined as three

Eulerian angles: longitude of the ascending node Ω being the precessional angle, inclination i being the nutational angle, and argument of periapsis ω being the rotational angle.

The SMBH of mass $M_\bullet$ dominates the gravitational potential considered in our model, its gravitational potential $\Phi_\bullet(r)$ is given by

$$\Phi_\bullet(r) = -\frac{\mathbb{G}M_\bullet}{r}. \tag{2.2}$$

Recent NIR observations (Schödel et al., 2003 and 2007) of the central spherical cusp of old stars show that the density profile of this cluster is described with a broken power-law profile (1.1). From the Poisson equation follows its potential with $M_{\rm sphe}/M_\bullet \geq 0$:

$$\Phi_{\rm sphe}(r) = \begin{cases} \dfrac{1}{(\alpha-2)\,r_{\rm sphe}}\,\mathbb{G}M_{\rm sphe}\left(\dfrac{r}{r_{\rm sphe}}\right)^{2-\alpha} & \text{for } \alpha \in [0;3)\setminus\{2\}, \\ \dfrac{\alpha-3}{r_{\rm sphe}}\,\mathbb{G}M_{\rm sphe}\ln(r) & \text{for } \alpha = 2. \end{cases} \tag{2.3}$$

The CND is modelled as an infinitely-thin homogeneous ring with a radius $R_{\rm CND}$. The potential of CND expressed in cylindrical coordinates (R, Z) then reads

$$\Phi_{\rm CND}(r) = -2\mathbb{G}\frac{M_{\rm CND}}{2\pi R_{\rm CND}}\sqrt{\frac{R_{\rm CND}}{R}}\,k\,\mathcal{K}(k), \tag{2.4}$$

$$\text{where } k^2 = \frac{4RR_{\rm CND}}{(R_{\rm CND}+R)^2+Z^2}, \tag{2.5}$$

and $\mathcal{K}(k)$ is the complete elliptic integral of the first kind:

$$\mathcal{K}(k) = \int_0^{\pi/2}\left(1-k^2\sin^2\theta\right)^{-1/2}\,\mathrm{d}\theta. \tag{2.6}$$

The CWS stellar disk is modelled as a set of test particles moving in the composed gravitational potential (2.1). While we consider the stars of the CWS stellar disk as the test particles, we neglect their mutual gravitational and non-gravitational interaction. The test particles form initially a planar structure and if they were under the influence of a central point mass only, they would form such a planar structure and would stay in such a structure forever. However, the presence of the two perturbing potentials $\Phi_{\rm CND}$ and $\Phi_{\rm sphe}$ causes a secular evolution of their orbital elements, which leads

to a spatial deformation (distortion and warp) of the initial planar structure. The magnitude of the deformation depends on the following set of parameters:

- parameters describing the $\Phi_{\rm CND}$: total mass of the CND $M_{\rm CND}$ and its radius $R_{\rm CND}$,
- parameters describing the $\Phi_{\rm sphe}$: total mass $M_{\rm sphe}$ of the spherical cusp inside a sphere of radius $r_{\rm sphe} = R_{\rm CND}$, its power-law profile index α,
- initial orbital elements of the test particle: the semi-major axis a_0, eccentricity e_0, inclination of the orbit i_0, argument of periapsis ω_0 and the longitude of the ascending node Ω_0.

2.2 Perturbation influence on the orbital elements

The orbit of a test particle moving in the potential of a point mass source with mass M is described by 6 orbital elements: the semi-major axis a, eccentricity e, inclination i, longitude of the ascending node Ω, argument of periapsis ω and the time of periapsis passage T_0. The orbital elements remain constant over the whole revolution. However, the presence of a perturbation to the central potential brings along a secular change of some of the orbital elements. For a given potential (2.1) the semi-major axis a is a constant of motion. We discuss the influence of an axi-symmetrical perturbation, a spherical perturbation, and a composition of both mentioned perturbations on the temporal evolution in the subsequent sections.

2.2.1 Axi-symmetric perturbation

One of the subjects of our investigation is the circum-nuclear disk. This molecular disk represents an axi-symmetric perturbation (2.4) to the Keplerian SMBH potential (2.2). The axi-symmetric perturbing potential causes a secular evolution of the orbital elements inclination i, eccentricity e, argument of periapsis ω and longitude of the ascending node Ω. This kind of secular evolution has been investigated by Kozai, 1962 and independently by Lidov, 1962. They were interested in the secular evolution of such a hierarchical triple system, especially in satellites with a high inclination and eccentricity moving under the influence of the Sun and Jupiter. They used the Hamiltonian perturbation theory as a powerful tool for investigation of such a hierarchical triple system.

The Hamiltonian perturbation theory allows the use of an approximative technique, known as the "averaging" technique. Description of this technique is e.g. in the textbook by Morbidelli, 2002. The "averaging" technique enables us to get rid of the short periodic changing angle, e.g. the mean anomaly, by virtue of the canonical transformation of Delaunay variables. We can consider an axially symmetric perturbation as orbit of a single mass point averaged over the fast changing angle, i.e. over the mean anomaly. Proper choice of canonical transformation enables us to rewrite the Hamiltonian $\mathcal{H}^\star_{\rm tot}$ as

$$\mathcal{H}^\star_{\rm tot}(\mathbf{p}^\star, \mathbf{q}^\star) = \mathcal{H}_\bullet(\mathbf{p}^\star) + \varepsilon\,\bar{\mathcal{H}}_1(\mathbf{p}^\star) + \varepsilon^2\,\mathcal{H}_2(\mathbf{p}^\star, \mathbf{q}^\star), \tag{2.7}$$

where $\mathcal{H}_\bullet$ is the unperturbed part, $\bar{\mathcal{H}}_1$ is a perturbation of the order of ε averaged over the fast changing angle and $\mathcal{H}_2$ is a perturbation of the order of ε^2, $\mathbf{p}^\star$ denotes the canonically transformed action and $\mathbf{q}^\star$ the angle variables.

Let us discuss the dynamics of an integrable system in $n = 3$ dimensions which is in general represented by the Hamiltonian $\mathcal{H}_\bullet(\mathbf{p})$, so is independent of the angles $\mathbf{q}$. The equations of motion read

$$\dot{p}_j = -\frac{\partial \mathcal{H}_\bullet}{\partial q_j}(\mathbf{p}) = 0, \quad \dot{q}_j = \frac{\partial \mathcal{H}_\bullet}{\partial p_j}(\mathbf{p}) \equiv \omega_j(\mathbf{p}), \quad 1 \le j \le n. \tag{2.8}$$

It follows from the equations of motion that the actions p_j are constants of motion and the angles q_j have constant frequencies ω_j.

A torus $\mathbf{T}^n$ is a $n-$dimensional manifold which admits n independent angles as a global coordinate system. In the motion described by (2.8), the angles circulate with constant frequencies on tori defined by $\mathbf{p} = \text{const.}$ The tori with $\mathbf{p} = \text{const.}$ (constants of motion) are invariant for the dynamics in the sense that the trajectory with the starting point on the torus will never leave the torus. The phase space is foliated in invariant tori, because every initial condition $\mathbf{p}_{(0)}$, $\mathbf{q}_{(0)}$ generates motion on the invariant torus. The motion of the angles on a torus depends on the frequencies $\omega_j(\mathbf{p})$. If the frequencies $\omega_j(\mathbf{p})$ admit $\mathbf{k} = (0, \ldots, 0)$ as a unique integer solution of the equation

$$\mathbf{k} \cdot \omega = \sum_{j=1}^{n} k_j\,\omega_j = 0, \quad \mathbf{k} \equiv (k_1, \ldots, k_n) \in \mathbb{Z}^n, \tag{2.9}$$

the motion densely covers the torus. Thus, the frequencies are said to be non-resonant and the motion is called quasi-periodic.

On the contrary, if equation (2.9) admits $n-1$ independent integer nonzero vectors $\mathbf{k}^1, \dots \mathbf{k}^n$, the motion on the torus is periodic. In this case it is easy to express the $n-1$ angles as periodic function functions of a unique angle. The frequencies are said to be completely resonant.

From now on we use e, i, ω and Ω as symbols for the averaged orbital elements, unless stated otherwise. The temporal evolution of the averaged orbital elements e, i, ω and Ω influenced by an axially perturbed potential has an oscillative pattern – see Fig. 2.1. The frequency of oscillations is directly proportional to the mass of the ring. The amplitude of the oscillation depends on the properties of the Φ_{CND} potential and on the orbital elements of the test particle. There are other integrals of motion besides the semi-major axis a. One of them is the quantity c_1 proportional to the z-component of the angular momentum:

$$c_1 = \sqrt{1-e^2}\cos i, \tag{2.10}$$

which is known as the Kozai integral. According to the "averaging" technique, the revolution-averaged value of the perturbation potential $\overline{\Phi}_{\mathrm{CND}}$ is also an integral of motion. These three integrals of motion represent a set of helpful tools for exploration of the oscillations of the orbital elements e, i and ω. Let us show the evolution of a stellar orbit in an evolutionary diagram in Fig. 2.2. In the polar coordinate grid, where e is the radial coordinate and ω represents the angular coordinate, we plot the isocontours of the one-revolution averaged $\overline{\Phi}$.

The Hamiltonian perturbation theory and the "averaging" technique enable us to split the expression of the Hamiltonian of the system into the unperturbed part and into the perturbed part, which are both time independent. Another reasonable assumption of the perturbation theory is that the contribution of the perturbed part to the Hamiltonian of the system is much smaller, almost negligible, than the unperturbed one. Thus, the dominance of the unperturbed, purely Keplerian, part of the Hamiltonian and the fact that $\overline{\Phi}$ is an integral of motion allow us to investigate the evolution of the averaged value of the perturbing potential $\overline{\Phi}_{\mathrm{CND}}$ along the Keplerian orbit. The initial conditions for integration of such a trajectory are given by a set of Keplerian orbital elements. The initial eccentricity e and argument of periapsis ω are given by the position of the trajectory in the evolutionary diagram. The time independence of the whole Hamiltonian enables us to choose an arbitrary value of the time of pericentre passage T_0 and of the longitude of the ascending node Ω. The semi-major axis a is constant in the evolutionary diagram, and so is the Kozai integral c_1, which determines the initial inclination i according to relation (2.10).

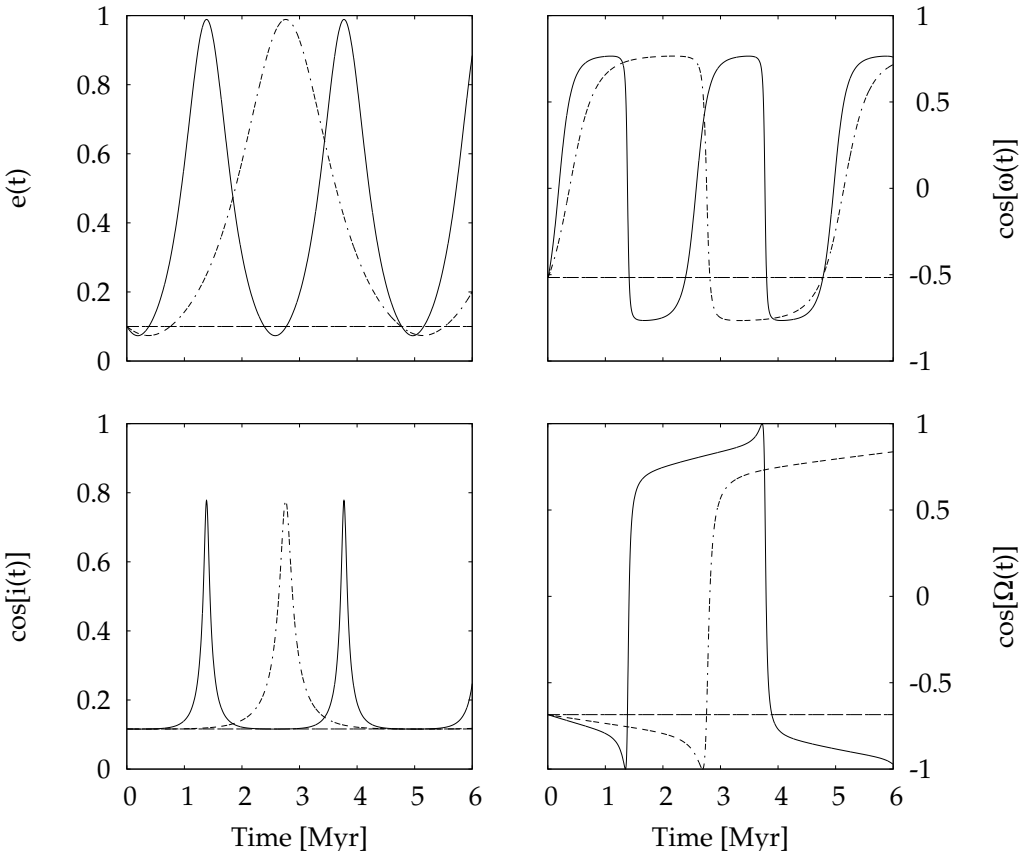

Figure 2.1: Comparison of the temporal evolution of the orbital elements of a test particle influenced by a Keplerian potential (dash line), or by an axially perturbed Keplerian potential with the perturbation mass $M_{\mathrm{CND}}/M_{\bullet} = 0.3$ (dash-dot line) or 0.6 (solid line) obtained by numerical integration of the exact equations of motion. Orbital elements of a test particle influenced by a purely Keplerian potential are constant. On the contrary, the presence of an axisymmetric perturbation causes oscillations of e, i, ω and Ω. The amplitude of oscillations is determined by the Φ_{CND} properties. The frequency of oscillations is directly proportional to the mass of the perturbation. Note the different period of Ω and the period of the other three orbital elements. Such temporal evolution was obtained by numerical integration of the exact equations of motion. In our simulations we used a Runge-Kutta integrator of the 4^{th} order with an adaptive stepsize control. The orbital elements shown in this Figure are the one-revolution averaged values obtained from the current positions and velocities by virtue of the Laplace method of coordinates determination.

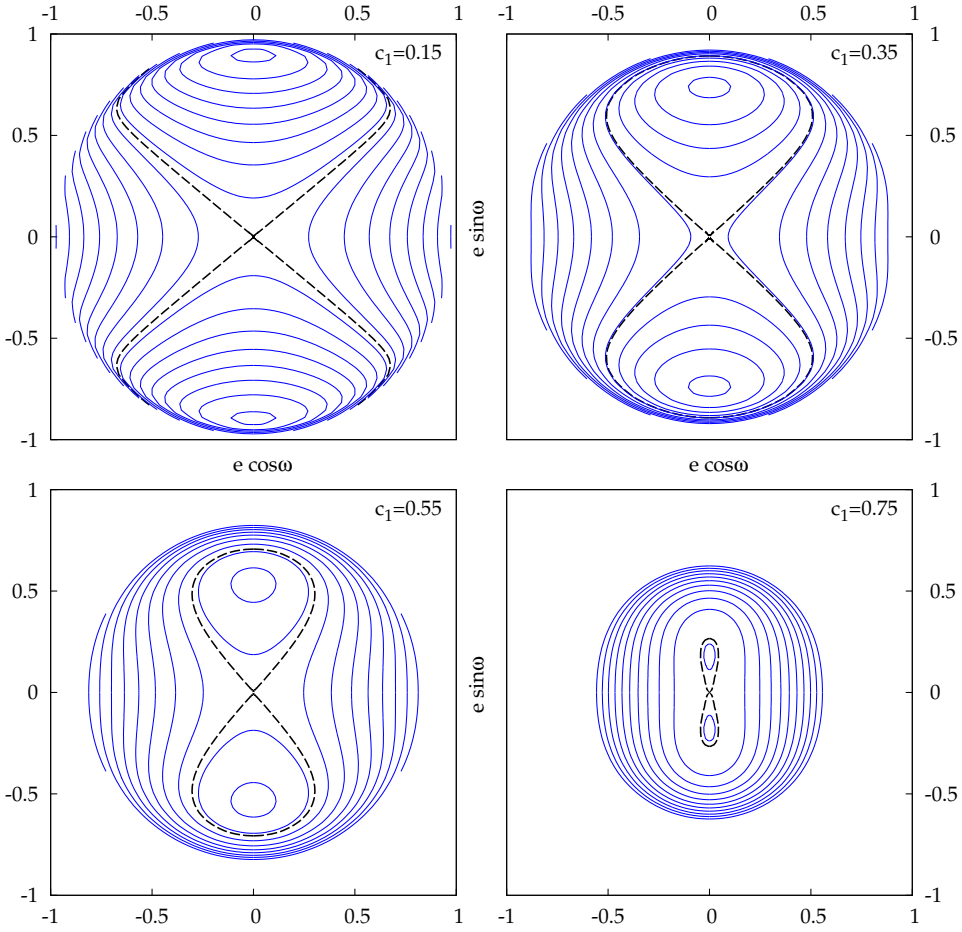

Figure 2.2: Evolutionary diagrams of a stellar orbit. The four panels show iso-contours of the averaged axisymmetric perturbing potential for a test particle with fixed $a = 0.04$ pc and for different values of $c_1 = 0.15, 0.35, 0.55, 0.75$. The polar coordinates are the eccentricity e (radial) and the argument of periapsis ω (angular coordinate) in these diagrams. Separatrix is depicted with a thick dash line. Note the decrease of the $e_{\max}$ with the increase of c_1.

The diagrams show properties of the orbital elements evolution listed below.

- Evolutionary diagram consists of two different regions: the librational region and the circulation region. In the librational region ω periodically oscillates in a limited range of values $\subset [0\,^\circ; 360\,^\circ)$, while in the circulation region it changes secularly over the whole $[0\,^\circ; 360\,^\circ)$ range.

- Value of $e_{\max}$ is not equal to 1, but according to the value of the Kozai integral c_1, the eccentricity ranges $e \in [e_{\min}; e_{\max}]$, where

$$e_{\max} = \sqrt{1 - c_1^2}. \tag{2.11}$$

- Maximal eccentricity $e_{\max}$ is reached when $\omega = 90\,^\circ$ or $270\,^\circ$. In these points the inclination reaches its minimal value $i_{\min}$. On the contrary, the minimal eccentricity $e_{\min}$ occurs when $\omega = 0\,^\circ$ or $180\,^\circ$, and the inclination reaches its maximal value $i_{\max}$.

- Amplitude $(e_{\max} - e_{\min})_\star$ of eccentricity change of the whole ensemble of possible trajectories is highest on the separatrix and damps down to zero with increasing distance from the separatrix. In the region of libration of ω the amplitude equals zero for two points with $\omega = 90\,^\circ$ or $270\,^\circ$ and $e = e_{\max}$. On the other hand, in the circulation region the points of zero amplitude form a circle with radius $e_{\max}$.

As the averaged $\overline{\Phi}$ is constant along the trajectory of the test particle, we can consider contours of $\overline{\Phi}$ as the evolutionary tracks of the stellar orbit. We show stellar tracks projected onto the evolutionary diagram in Fig. 2.3. The tracks were obtained by integration of exact equations of motion of a test particle in the potential of the SMBH (2.2) axially perturbed by an infinitely-thin ring (2.4). We highlight two characteristic trajectories representative of two families of orbits, one family represents a particle residing in the librational region, the other one belongs to the circulation region family.

Another way of investigation of the temporal evolution of the orbital elements e, i, ω and Ω is the solution of the quadrupole approximation to the exact equations of motion. The multipole expansion of Hamiltonian is commonly used in the exploration of a multiple hierarchical system. Kozai, 1962, Lidov & Ziglin, 1976, and Kiseleva et al., 1998 used the quadrupole approximation for investigating a triple hierarchical system.

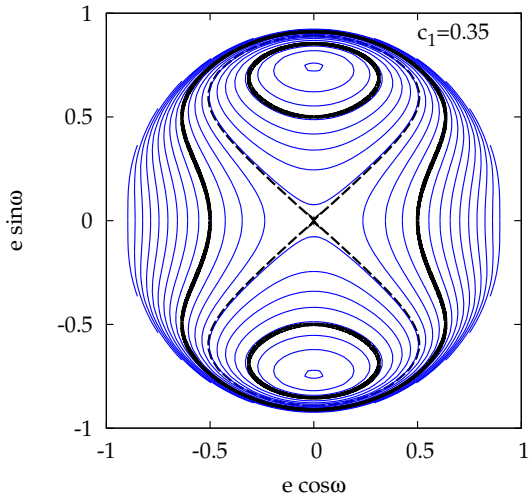

Figure 2.3: Stellar trajectory highlighted in the evolutionary diagram. The trajectory was obtained by direct integration of the equations of motion of a test particle with $a = 0.04$ pc ($R_{\rm CND}/a = 45$) for $c_1 = 0.35$ influenced by an axisymmetric potential (2.4) with $M_{\rm CND}/M_\bullet = 0.05$. The dash line denotes separatrix, with the libration region inside the separatrix lobes, and the circulation region outside the lobes. The thick lines denote a stellar orbit, one in the librational region, another one in the circulation region.

The quadrupole equations read

$$T_{\rm K}\frac{{\rm d}e}{{\rm d}t} = +\frac{5}{2}e\sqrt{1-e^2}\sin^2(i)\sin(2\omega), \tag{2.12}$$

$$T_{\rm K}\frac{{\rm d}i}{{\rm d}t} = -\frac{5}{2}\frac{e^2}{\sqrt{1-e^2}}\cos(i)\sin(i)\sin(2\omega), \tag{2.13}$$

$$T_{\rm K}\frac{{\rm d}\omega}{{\rm d}t} = \frac{1}{\sqrt{1-e^2}}\left\{2(1-e^2)+5\sin^2(\omega)\left[e^2-\sin^2(i)\right]\right\}, \tag{2.14}$$

$$T_{\rm K}\frac{{\rm d}\Omega}{{\rm d}t} = -\frac{\cos(i)}{\sqrt{1-e^2}}[1+4e^2-5e^2\cos^2(\omega)], \tag{2.15}$$

where

$$T_{\rm K} = \frac{4}{3}\left(\frac{M_{\rm CND}}{M_\bullet}\right)^{-1}\left(\frac{a}{R_{\rm CND}}\right)^{-3}\frac{P_{\rm orb}}{2\pi} \tag{2.16}$$

is the characteristic timescale of the Kozai effect and the orbital period $P_{\rm orb}$ reads

$$P_{\rm orb} = 2\pi\sqrt{\frac{a^3}{\mathbb{G}M_\bullet}}. \tag{2.17}$$

Two integrals of motion follow from these equations, the Kozai integral c_1 given by (2.10), and

$$c_2 = \left[2(1-e^2) + 5e^2 \sin^2(\omega)\right] \sin^2(i), \tag{2.18}$$

which is proportional to the averaged value of the perturbing potential $\overline{\Phi}$ (Carruba et al., 2002). The detailed derivation of the quadrupole equations (2.12)-(2.15) is shown in Appendix A. Let us focus on the quadrupole equations with emphasis on the mutual dependence of the four orbital elements e, i, ω and Ω. From (2.12)-(2.14) it is obvious that the temporal evolution of e, i and ω is mutually coupled. However, none of these three orbital elements depends on the fourth orbital element Ω. On the contrary, from (2.15) follows that Ω depends on those three orbital elements and is independent of its value. This kind of coupled dependence is important for preservation or destruction of any planar structure, e.g. the investigated clockwise stellar disk. Since the e, i and ω evolutions are mutually coupled and Ω stays apart, we can expect that characteristic timescales of the change of e, i and ω will be similar, but the characteristic timescale of Ω could be different, as we show in Section 2.2.3. Thus, the exploration of Ω characteristic timescale, period P_Ω, is the key to the limitation of the mass of the circum-nuclear disk.

2.2.2 Spherical perturbation

In this section, we investigate the influence of the spherical cusp on the temporal evolution of the orbital elements. The spherical perturbation (2.3) to the central Keplerian potential causes an apsidal precession. The precession rate is directly proportional to the mass of the spherical perturbation.

We performed a set of direct numerical integrations of the equations of motion of a test particle in order to probe the dependence of the precession rate on the total mass $M_{\rm sphe}$ of the spherical perturbation and on the power-law index α of the power-law mass-density distribution. The numerical result is shown in Fig. 2.4. Ivanov et al., 2005 have expressed the precession rate per one revolution $\delta\omega$ of a stellar orbit induced by the gravitational field of a stellar cusp as a function of the profile α and the total mass $M_{\rm sphe}$ of the cusp, the stellar semi-major axis a and the eccentricity e:

$$\delta\omega = \frac{2}{2-\alpha}\frac{M_{\rm sphe}}{M_\bullet}\left(\frac{a}{R_{\rm sphe}}\right)^{3-\alpha}\frac{\sqrt{1-e^2}}{e} \times$$

$$\times \left[(7-2\alpha)\, e \left(1-e^2\right)^{5/2-\alpha} \mathcal{A} + (4-\alpha) \quad \left(1-e^2\right)^{7/2-\alpha} \mathcal{B} \right], \qquad (2.19)$$

$$\text{where} \quad \mathcal{A} \equiv \int_0^{\pi} \frac{\mathrm{d}\varphi}{(1+e\cos\varphi)^{4-\alpha}}, \qquad (2.20)$$

$$\mathcal{B} \equiv \int_0^{\pi} \frac{\cos\phi\, \mathrm{d}\varphi}{(1+e\cos\varphi)^{5-\alpha}}. \qquad (2.21)$$

The precession rate $\delta\omega$ can be expressed in terms of elliptic integrals for several half-integer values of α. $\delta\omega$ for these values is shown in Fig. 2.4. We show that for a given mass $M_{\rm sphe}$, the apsidal precession of the same test particle with a given semi-major axis a can differ by an order of magnitude, depending on the power-law index α. For a detailed derivation of (2.19) see Ivanov et al., 2005.

We show the temporal evolution of the eccentricity e, argument of periapsis ω, inclination i and longitude of the ascending of node Ω in Fig. 2.5. Since the orbital elements a, e, i and Ω remain constant and the precession of ω does not scatter the spatial structure, the spherical cusp cannot destroy the planar stellar disk.

Let us now discuss the effect of the ω precession on the evolution of the orbital elements of a test particle influenced by the composed potential (2.1). Ivanov et al., 2005 investigated a tidal disruption of stars in a stellar cluster in the centre of a galaxy. They assumed that stars are moving in a potential dominated by the SMBH, axially perturbed by a secondary black hole and spherically perturbed by a spherical cusp of stars. They modified the quadrupole equation for ω (2.14) by adding the precession term:

$$T_{\rm K}\frac{\mathrm{d}\omega}{\mathrm{d}t} = \frac{1}{\sqrt{1-e^2}} \left\{ 2(1-e^2) + 5\sin^2(\omega) \left[e^2 - \sin^2(i) \right] \right\} - \kappa\sqrt{1-e^2}, \qquad (2.22)$$

where the last term is the precession term:

$$\begin{aligned} \kappa &= K \left(\frac{T_{\rm K}}{P_{\rm orb}}\right) \left(\frac{M_{\rm sphe}}{M_\bullet}\right) \left(\frac{a}{R_{\rm CND}}\right)^{3-\alpha} \frac{P_{\rm orb}}{2\pi} \\ &= \frac{2^{4-\alpha}}{3\sqrt{\pi}} \frac{\Gamma\left(\frac{5}{2}-\alpha\right)}{\Gamma(3-\alpha)} \frac{M_{\rm sphe}}{M_{\rm CND}} \left(\frac{a}{R_{\rm CND}}\right)^{-\alpha}, \end{aligned} \qquad (2.23)$$

where for small e

$$K = 2^{3-\alpha}\sqrt{\pi}\, \frac{\Gamma\left(\frac{5}{2}-\alpha\right)}{\Gamma(3-\alpha)}, \qquad (2.24)$$

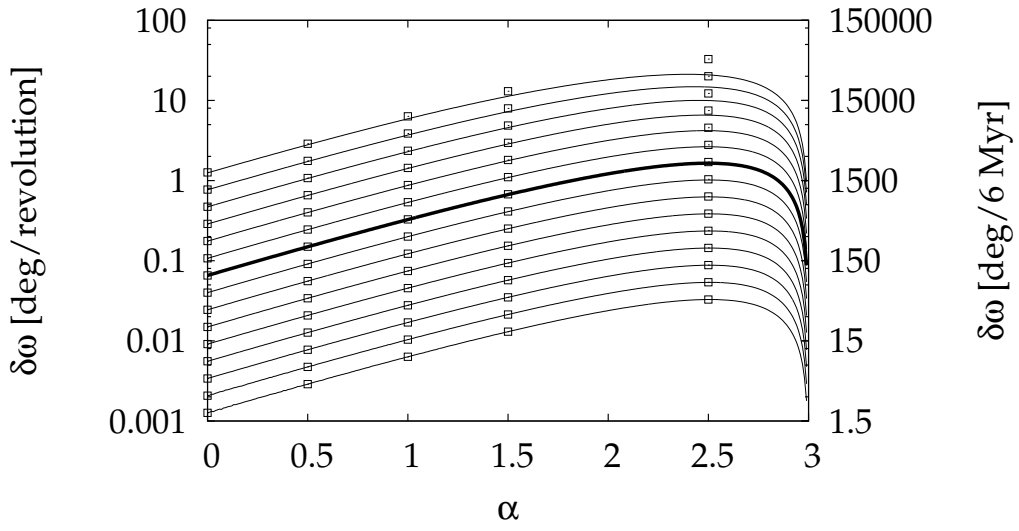

Figure 2.4: Apsidal precession as a result of direct numerical integration of equations of motion of a test particle influenced by the central potential field perturbed by a spherical perturbation compared to Ivanov et al., 2005 formula (2.19) result for several special values of α. Different lines represent different values of $M_{\rm sphe}$ inside the sphere with radius $R_{\rm sphe} = 1.8$ pc, $M_{\rm sphe} = 10^{-3}\,M_\bullet$ to $1\,M_\bullet$ from the bottom to the top, with a logarithmic step. The thick line denotes $M_{\rm sphe} = 0.05\,M_\bullet$, which we further discuss in Section 2.2.3. The cusp with a mass higher than $M_{\rm sphe}/M_\bullet \approx 0.14$ (fifth line from the top) induces a lower apsidal precession rate than the value expected from formula (2.19). This discrepancy between the numerical result and the theoretical formula rose probably from the fact that above a certain mass the cusp is too heavy to be treated as a perturbation.

e.g. $K(1.75) = 5.70$. Let us compare the frequency of ω due to the axially symmetric perturbation $\nu_{\rm quad}$ and the frequency due to the apsidal precession $\nu_{\rm sphe}$:

$$\nu_{\rm quad} \equiv \frac{1}{T_{\rm K}}\frac{1}{\sqrt{1-e^2}}\left\{2(1-e^2)+5\sin^2(\omega)\left[e^2-\sin^2(i)\right]\right\}, \quad (2.25)$$

$$\nu_{\rm sphe} \equiv \frac{1}{T_{\rm K}}\kappa\sqrt{1-e^2}. \quad (2.26)$$

The characteristic timescale of Kozai oscillations $T_{\rm K}$ expressed in characteri-

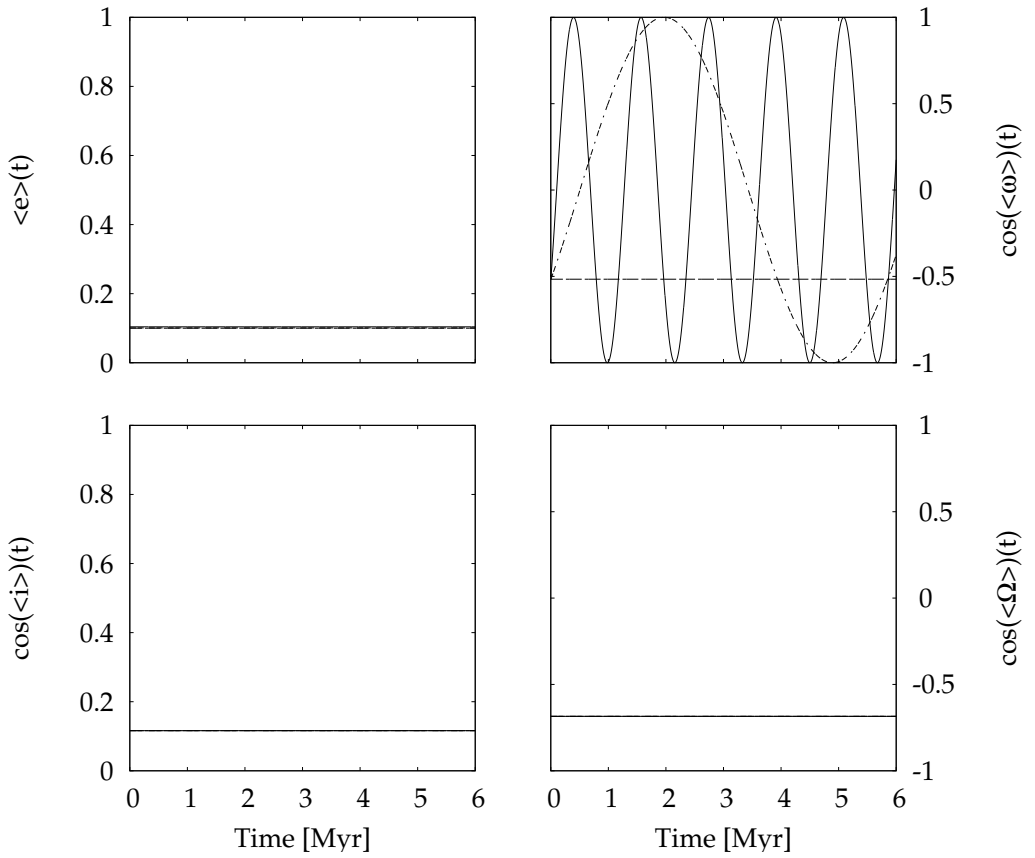

Figure 2.5: Temporal evolution of the averaged orbital elements of a test particle influenced by a spherically perturbed potential of $M_{\text{sphe}}/M_\bullet = 0$, 0.0135 and 0.0675. The semi-major axis $a = 0.2$ pc is a constant of motion. The averaged eccentricity e, the averaged inclination i and the averaged longitude of the ascending node Ω also remain constant. The presence of the spherical perturbation exposes its power in the periodic changes of ω, the frequency of changes is directly proportional to the mass of the spherical perturbation, as we have seen in (2.19). The change in the averaged ω itself does not scatter the spatial structures – every disk-like structure remains disk-like while influenced just by the spherical potential.

stic values of parameters of our model reads

$$\left(\frac{T_{\mathrm{K}}}{\mathrm{Myr}}\right) = 0.5 \left(\frac{M_{\mathrm{CND}}}{M_\bullet}\right)^{-1} \left(\frac{M_\bullet}{3.5\times10^6\,M_\odot}\right)^{-1/2} \times \times \left(\frac{a}{0.24\,\mathrm{pc}}\right)^{-3/2} \left(\frac{R_{\mathrm{CND}}}{1.8\,\mathrm{pc}}\right)^{+3} \tag{2.27}$$

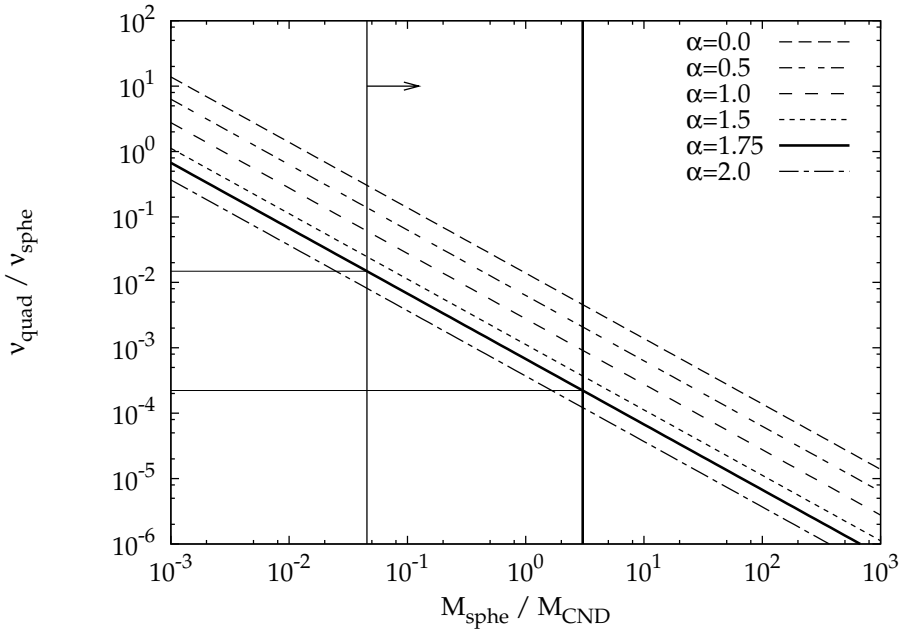

Figure 2.6: $\nu_{\mathrm{quad}}/\nu_{\mathrm{sphe}}$ for a test particle with $a = 0.24$ pc as a function of $M_{\mathrm{sphe}}/M_{\mathrm{CND}}$ and α. The thick vertical line represents $M_{\mathrm{sphe}}/M_{\mathrm{CND}}$ according to current observations, while the thin vertical line with arrow represents $M_{\mathrm{sphe}}/M_{\mathrm{CND}} = 1/22$, the lower limit of the $M_{\mathrm{sphe}}/M_{\mathrm{CND}}$ ratio interval for which ω circulates through the whole $[0\,^\circ; 360\,^\circ]$ range.

We show the possible range of $\nu_{\mathrm{quad}}/\nu_{\mathrm{sphe}}$ for a test particle with $a = 0.24$ pc in Fig. 2.6. Since (2.24) is valid only for small e, we expect i to be close to $90\,^\circ$ due to the Kozai integral c_1 constraint and the characteristic behaviour of i and e described in Fig. 2.2 (evolutionary diagrams). Thus, we focus our interest on $i = 88\,^\circ$, which is close to $90\,^\circ$. For this inclination, the amplitude of $\nu_{\mathrm{quad}}/\nu_{\mathrm{sphe}}$ does not exceed a few percent of the mean $\nu_{\mathrm{quad}}/\nu_{\mathrm{sphe}}$ value for any ω. We plot $\nu_{\mathrm{quad}}/\nu_{\mathrm{sphe}}$ as a function of $M_{\mathrm{sphe}}/M_{\mathrm{CND}}$ for different power-law profiles α of the spherical cusp. Our simulations show that for $\nu_{\mathrm{quad}}/\nu_{\mathrm{sphe}} \lesssim 0.05$ the ω circulates, even though

without the cusp it would just librate. The effect of the temporal evolution of ω on the temporal evolution of e, i and Ω is discussed in the following section.

2.2.3 Composed perturbation

We introduced the ratio $\nu_{\rm quad}/\nu_{\rm sphe}$ as a tool for the evaluation of the strength of the spherical component of our model of the Galactic Centre in terms of the temporal evolution of ω. However, for the model with a very light spherical cusp ($M_{\rm CND}/M_{\rm sphe} \gtrsim 20$) we cannot use this criterion for the comparison of frequency due to a typical non-linear temporal evolution. Nevertheless, the strength parameter $\nu_{\rm quad}/\nu_{\rm sphe} \lesssim 0.05$ helps us limit the set of the model parameters for which ω evolves very fast in time, thus e and i oscillate very fast and with amplitudes of a few per mille to a few percent, so that we can consider them constant.

In conclusion, the presence of even a light spherical perturbation together with an axi-symmetric perturbation with $M_{\rm CND}/M_{\rm sphe} \approx 20$ results in the dominance of the apsidal precession term (2.26) over the quadrupole term (2.25). The apsidal precession also changes the qualitative behaviour of ω. The presence of a relatively light spherical perturbation $M_{\rm CND}/M_{\rm sphe} = 4.5$ results in an enlargement of the inner circulation region and a contraction of the libration region around the poles of the evolutionary diagram, as we show in the top panels of Fig. 2.7. Adding the spherical perturbation causes more than four times higher frequency of ω compared to the frequency in the axially perturbed model. This change of the temporal ω behaviour affects temporal evolution of e, i and Ω. The apsidal precession significantly damps the amplitude and increases the frequency of e and i oscillations. Since the temporal evolution of e, i and ω cannot result in a deformation of the planar structure, the most important qualitative behaviour for the deformation of the stellar disk is that of Ω. For the model of the Galactic Centre with both perturbations and $M_{\rm CND}/M_{\rm sphe} \lesssim 20$, Ω changes *linearly* with time instead of its quadrupole-like behaviour (see Fig. 2.7), for $i \leq 90^\circ$ Ω linearly decreases with time, for $i > 90^\circ$ it linearly increases with time.

We show the characteristic temporal evolution of 2 test particles influenced by realistic perturbations due to the observations: an axial one with the mass-ratio $M_{\rm CND}/M_\bullet = 0.33$ and a spherical one with $M_{\rm sphe}/M_\bullet = 1$ in Fig. 2.8. We show that for such two test particles the period of the orbital elements e, i and ω is ≈ 0.1 Myr, while the period of Ω is ~ 215 Myr.

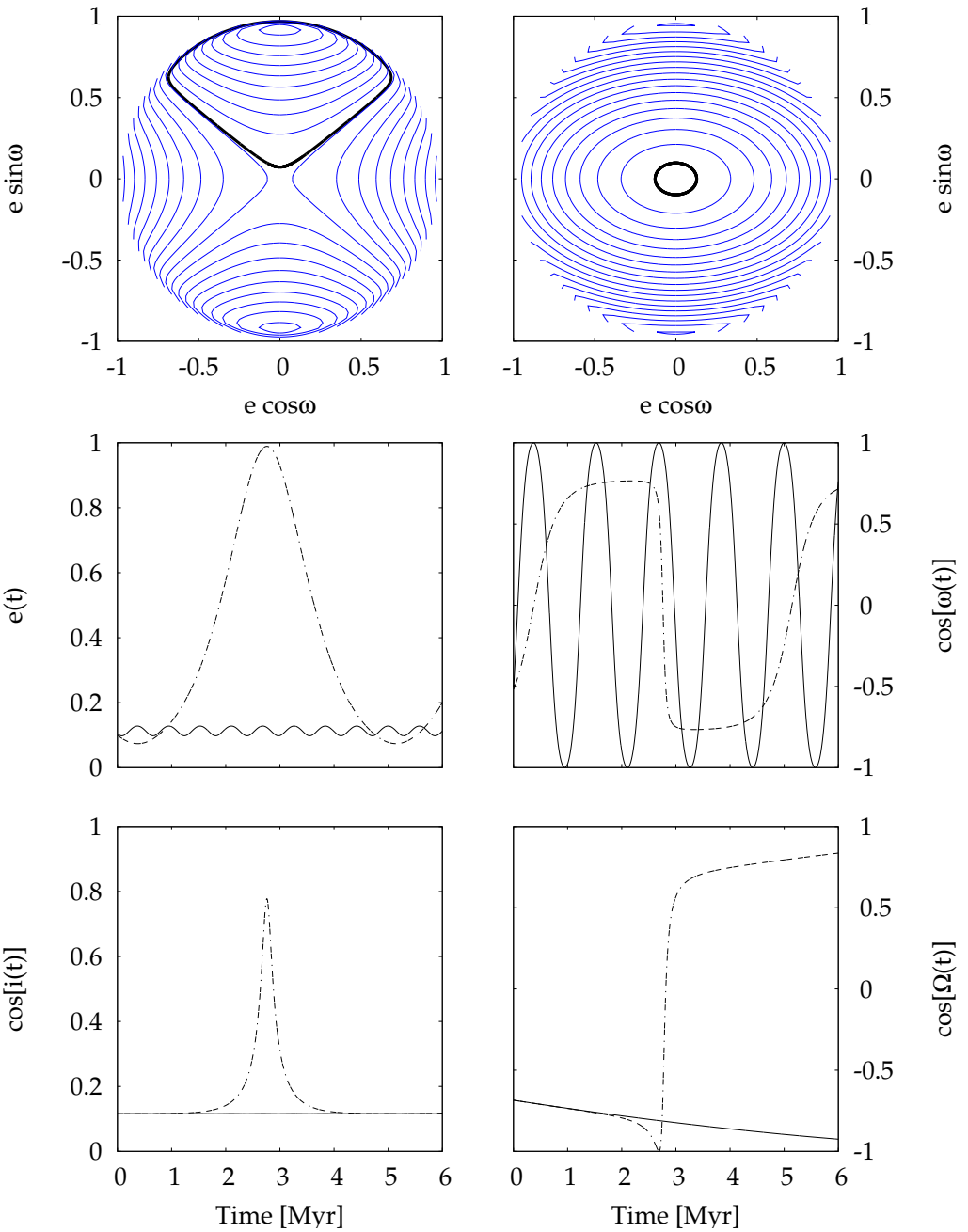

Figure 2.7: Comparison of the orbital elements evolution for a test particle with $a = 0.2$ pc influenced by an axially perturbed potential ($M_{\rm CND}/M_\bullet = 0.3$) without a cusp (dash-dot) and with a spherical cusp (solid) with $M_{\rm CND}/M_{\rm sphe} = 4.5$. The top left panel shows isocontours of $\overline{\Phi}_{\rm CND}$ for such a particle, the top right panel shows $\overline{\Phi}_{\rm CND+sphe}$. Note that the spherical perturbation causes an increase of the frequency of oscillations and the amplitude damping for e, i.

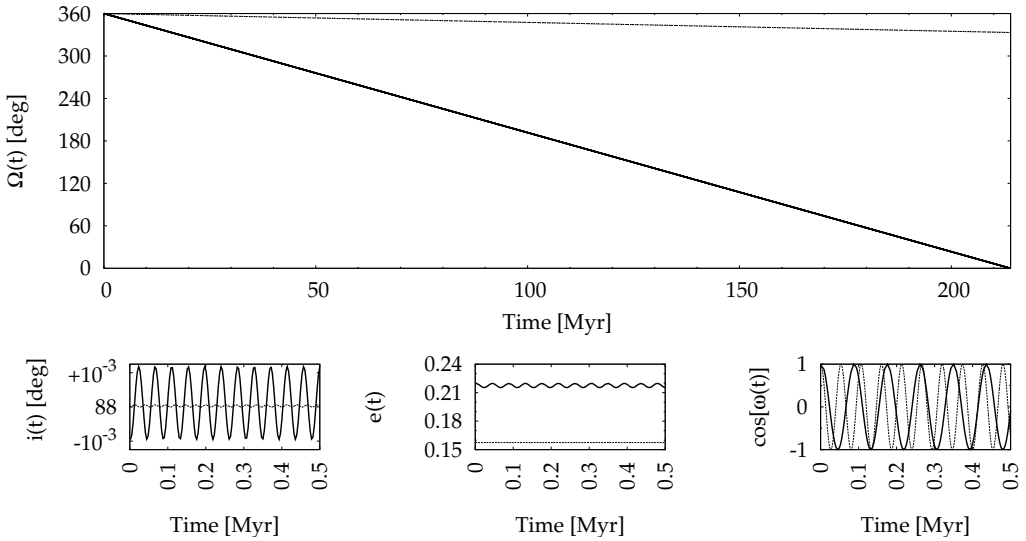

Figure 2.8: Temporal evolution of Ω, i, e and ω for two test particles with $a = 0.24$ pc (thick line) and $a = 0.04$ pc (thin line) in a realistic composed potential with $M_{\rm CND}/M_\bullet = 0.33$ and $M_{\rm sphe}/M_\bullet = 1$. Note that the characteristic timescale of change of e, i and ω is ~ 0.1 Myr, while the Ω characteristic timescale is much longer ~ 215 Myr.

2.2.4 Consequences of P_Ω

Since the frequency of ω change for $M_{\rm CND}/M_{\rm sphe} \lessapprox 20$ is quite high compared to the frequency of Ω, it enables us to average the quadrupole equation for Ω (2.15) over ω. Since i and e remain constant (at a first approximation) for fast changes of ω, the bracket-term in

$$T_{\rm K}\,\frac{{\rm d}\Omega}{{\rm d}t} = -\frac{\cos(i)}{\sqrt{1-e^2}}\left[1+4e^2-5e^2\cos^2(\omega)\right]$$

becomes constant and the term $\frac{\cos(i)}{\sqrt{1-e^2}}$ becomes also time-independent. Therefore, the "averaged" equation (2.15) simplifies as

$$\frac{{\rm d}\Omega}{{\rm d}t} = -\frac{1}{T_{\rm K}}\frac{1+\frac{3}{2}e^2}{\sqrt{1-e^2}}\cos(i) = \frac{\text{const.}}{T_{\rm K}}. \tag{2.28}$$

Since Ω changes linearly with time, we convert this rate to a periode $P_\Omega|_{\rm quad}$:

$$P_\Omega|_{\rm quad} = T_{\rm K}\,\frac{2\pi}{\text{const.}} \tag{2.29}$$

$$= \frac{4}{3}\left(\frac{M_{\rm CND}}{M_\bullet}\right)^{-1}\left(\frac{a}{R_{\rm CND}}\right)^{-3}\frac{P_{\rm orb}}{|\cos(i)|}\,\frac{\sqrt{1-e^2}}{1+\frac{3}{2}e^2}. \tag{2.30}$$

Employing (2.27) and inserting characteristic values of parameters, $P_\Omega|_{\rm quad}$ reads

$$\left(\frac{P_\Omega|_{\rm quad}}{\rm Myr}\right) = 95 \left(\frac{M_{\rm CND}}{M_\bullet}\right)^{-1} \left(\frac{M_\bullet}{3.5\times10^6\,M_\odot}\right)^{-1/2} \left(\frac{a}{0.24\ {\rm pc}}\right)^{-3/2} \times \times \left(\frac{R_{\rm CND}}{1.8\ {\rm pc}}\right)^{+3} \frac{|\cos(88\,^\circ)|}{|\cos(i_0)|} \frac{\sqrt{1-e^2}}{1+\frac{3}{2}e^2}. \quad (2.31)$$

In order to confirm P_Ω given by (2.30) we ran a set of numerical simulations, where we integrated exact equations of motion of a test particle in our Galactic Centre model. We were interested in the dependencies on parameters describing the Galactic Centre model and the orbit of a test particle $P_\Omega(a_0,\, e_0, i_0, \omega_0, \Omega_0; M_{\rm CND}, R_{\rm CND}; M_{\rm sphe}, \alpha; M_\bullet)$. We have found that P_Ω indeed is described by (2.30). We compare the analytic result (2.30) with results from numerical integrations of the exact equations of motion in Fig. 2.9. We plot isocontours of the surface $\Delta\Omega_{(6\ {\rm Myr})}(|\cos(i_0)|, M_{\rm CND})$ for a test particle with $a = 0.24$ pc in Fig. 2.9. As we show in this Figure, the analytic formula (2.30) is consistent with numerical results for $|\cos(i_0)| \in [\cos(89.5\,^\circ); \cos(40\,^\circ)]$. For $|\cos(i_0)| \gtrsim \cos(40\,^\circ)$ the analytic formula overestimates the $\Delta\Omega$ value obtained from the solution of the exact equations of motion by a few percent. For $|\cos(i_0)| \lesssim \cos(89.5\,^\circ)$ the analytic formula overestimates the numerical result by $\approx 10\%$. Considering the errors of the determination of the angle between the normal vector to the circum-nuclear disk and that to the clockwise stellar disk, we can conclude that the analytic formula (2.30) gives a sufficiently accurate estimate of the Ω precession for particles with an inclination from the range of the observed inclinations and far beyond.

Since Ω changes linearly with time, the period P_Ω can be converted into $\Omega(t)$ as follows

$$\Omega(t) = \Omega_{(t)} = \begin{cases} \Omega_{(0)} - 360\,^\circ \times \dfrac{t}{P_\Omega} & \text{for } i_0 \le 90\,^\circ, \\ \Omega_{(0)} + 360\,^\circ \times \dfrac{t}{P_\Omega} & \text{for } i_0 > 90\,^\circ, \end{cases} \quad (2.32)$$

where the subscript $_{(t)}$ denotes the time dependence.

Let us recapitulate the most significant dependencies of Ω:

$$\Delta\Omega_{(t)} \equiv \Omega_{(t)} - \Omega_{(0)} \propto \left(\frac{M_{\rm CND}}{M_\bullet}\right)^{+1} a^{+3/2} \cos(i_0) \quad (2.33)$$

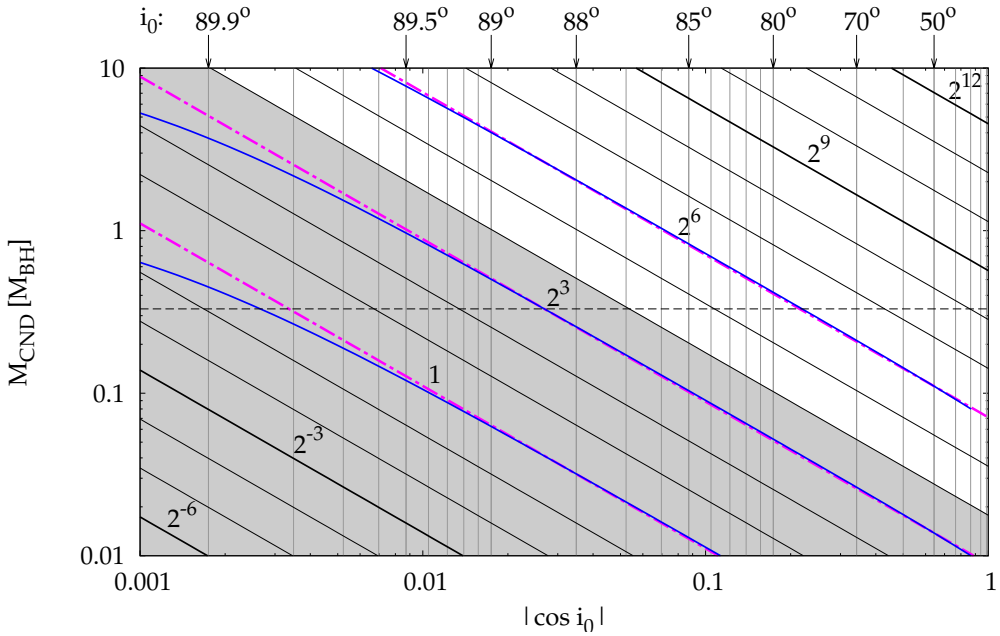

Figure 2.9: Isocontours of the surface $\Delta\Omega_{(6\ \mathrm{Myr})}(|\cos(i_0)|, M_{\mathrm{CND}})$ for a test particle with $a = 0.24$ pc. The isocontours are straight diagonal lines labelled by the po-wers of 2 in units of degrees per 6 Myr. The slopes of isocontours are given by formula (2.30). The three slightly curved thick lines are numerically obtained isocontours of the Ω precession. The formula (2.30) gives us a very accurate estimate of the Ω precession (compared to the Ω precession obtained by a numerical integration of the exact equations of motion) for initial inclinations $i_0 \in [40°; 89.5°]$. This range is sufficient according to the observed inclinations of the clockwise disk stars $i \approx 89°$. The vertical lines denote the initial inclinations from right to left: 0 to 70° with step 10°; 80° to 88° with step 1° and 89.0° to 89.9° with step 0.1°. The horizontal line denotes the current mass estimate by Christopher et al., 2005. Note the shaded half-plane below the $\Omega = 16°$ per 6 Myr, which restricts the possible i_0-M_{CND} values due to the current NIR observations of the clockwise stellar disk, as we discuss in Chapter 3.

Consider a set of test particles moving in the model (2.1) of the Galactic Centre. The model is described i.a. by the mass of the axi-symmetric perturbation M_{CND}. Thus, the direct proportionality between Ω and M_{CND} suggests that for some masses of CND the precession is too high to preserve the disk-like structure of the stellar disk. This enables us to exclude the half-plane given by $\Delta\Omega_{(t)} > \Delta\Omega_{\mathrm{crit}}$ from our considerations, as we show in Fig. 2.9.

Let us discuss the precession of Ω in the case of a set of test particles moving in a specific model of the Galactic Centre (2.1) with a given $M_\bullet$, M_{CND} and M_{sphe}, R_{CND} and α. Since the dependence on the orbital elements e, ω and T_0 are insignificant for our discussion, we focus only on the dependence on a and i_0.

According to the NIR observations by Paumard et al., 2006, the outer part of the stellar disk is worse defined as a planar structure. Thus, we are concerned just with the inner part of the stellar disk, i.e. the part with $a \in [0.04; 0.24]$ pc. The dependence on the semi-major axis a

$$\Delta\Omega_{(t)} \propto a^{+3/2}$$

is quite strong and can remarkably warp the stellar disk. Moreover, it tells us that a test particle with $a = 0.24$ pc undergoes a $15\times$ larger change of Ω than a particle with $a = 0.04$ pc, assuming these two particles had such initial inclinations that absolute values of their cosines were equal.

Let us consider two test particles with the same semi-major axes a moving in the same model of the Galactic Centre, but with different initial inclinations. While

$$\Delta\Omega_{(t)} \propto \cos(i_0),$$

the $\cos(i_0)$ factor permits a difference in the Ω precession by the order of several magnitudes, depending on i_0 values. It is a very distinctive factor for inclinations close to $90\,^\circ$, where a small change of i_0 causes several orders of magnitude large changes of $\cos(i_0)$, and less important for inclinations close to $0\,^\circ$ or $180\,^\circ$. Thus, a combination of characteristic values of a and i_0 of the test particles from the set representing the stellar disk are the key to the exploration of the deformation of the stellar disk in a given Galactic Centre model, i.e. for fixed values of parameters describing (2.1). On the contrary, the other orbital elements such as e, ω, Ω and T_0 and power-law profile of the spherical cusp α are less important parameters for the Ω precession, as well as for the stellar disk deformation.

3 On the deformation of stellar disk

In this Chapter we discuss consequences of the application of the knowledge of the period P_Ω on the exploration of the stellar disk deformation. In the first section we formulate a criterion for the disk deformation due to the cone of angular momentum vectors for all test particles from the disk. This criterion is modified in the second section for the purposes of the investigation of the angular momentum cone of particles at the outer margin of the considered part of the stellar disk. In the third section we discuss suitability of the criterion of the projection of the angular momentum to the line-of-sight direction proposed by Genzel et al., 2003.

3.1 Cone of angular momentum vectors of the whole stellar disk

In Chapter 2, we described the qualitative behaviour of the orbital elements of a test particle moving in our model (2.1) of the Galactic Centre, consisting of a super-massive black hole, an axially symmetric and a spherical perturbation. We have shown that the axially symmetric perturbation causes oscillations in e, i, ω and Ω. We have shown that the presence of even a light spherical perturbation causes an apsidal precession, which attenuates the amplitudes of the e and i oscillations appearing in the axially perturbed potential, so we can treat them as constant in time. Moreover, the apsidal precession rate results in a linear temporal evolution of Ω. We introduced the period of the Ω precession in equation (2.30).

In investigation of the deformation of the stellar disk, we assume that the stellar disk is a stable structure for 6 Myr, i.e. the timespan equal to the age of the stars as given by observations.

First, let us define Criterion 1, which gives us an estimate whether the disk is deformed or not, based on our knowledge of P_Ω from (2.30).

> **Criterion 1.** *The stellar disk has lost its initial planar structure, i.e. is deformed, if* $\Delta\Omega_{\max}$ *is larger than a critical value* $\Delta\Omega_{\text{crit}}$.

This Criterion has been expressed already in Section 2.2.4 and it is visualised in Fig. 2.9, where we shaded the half-plane of the possible $[i_0; M_{\mathrm{CND}}]$ pairs for a test particle with $a = 0.24$ pc, which fulfil Criterion 1 for $\Delta\Omega_{\mathrm{crit}} = 16\,^\circ$. Let us assume that the disk particles have inclinations from a range $i \in [i_{\mathrm{min}}; i_{\mathrm{max}}] \subset [0\,^\circ; 90\,^\circ]$. [1] Then the largest precession of Ω occurs for the particles at the outer margin of the considered disk – let us denote them by $a_{[6]} = 0.24$ pc $= 6''$ from now on – with $i = i_{\mathrm{min}}$. In contrast, the smallest precession of Ω occurs for particles at the innermost part of the stellar disk – let us denote them by $a_{[1]} = 0.04$ pc $= 1''$ – with the inclination $i = i_{\mathrm{max}}$.

However, in this Section we formulate another Criterion, which brings into play the maximal amount of information we know from the temporal evolution of the orbital elements. Criterion 2 concerns the cone of angular momentum vectors – hereafter denoted as the Cone – of all the test particles from the stellar disk for the description of the disk deformation. The definition of a unit angular momentum vector of a test particle with inclination i and longitude of the ascending of node Ω at time t reads

$$\mathbf{L}_{(t)} = \begin{pmatrix} +\sin[i_{(t)}]\ \sin[\Omega_{(t)}] \\ -\sin[i_{(t)}]\ \cos[\Omega_{(t)}] \\ +\cos[i_{(t)}] \end{pmatrix}. \tag{3.1}$$

Knowledge of $\Omega(t, a, i_0, M_{\mathrm{CND}}, \ldots)$ from (2.32) and the initial distribution of inclinations enables us to reconstruct the Cone at an arbitrary time $t > t_0$ and evaluate the disk deformation in terms of the opening angle of this Cone.

This tells us that the opening angle of the Cone is determined by the angle Δ between the two "furthest" particles, particle with $(a = 0.04\,\mathrm{pc},\ i_{\mathrm{max}})$ denoted with the subscript $_{[1]}$, and a particle with $(a = 0.24$ pc, $i_{\mathrm{min}})$ denoted with the subscript $_{[6]}$:

$$\cos[\Delta_{(t)}] \equiv \mathbf{L}_{(t)[1]} \cdot \mathbf{L}_{(t)[6]}. \tag{3.2}$$

It follows from the Δ definition that $\Delta \in [0\,^\circ; 180\,^\circ]$. We have searched for the dependence of the Cone opening angle Δ on the initial distribution of $\Omega_0 \in [\Omega_{0,\,\mathrm{min}}; \Omega_{0,\,\mathrm{max}}]$. We have obtained the largest opening angle for a single value of Ω_0, i.e. for $\Omega_0 = \Omega_{0,\,\mathrm{min}} = \Omega_{0,\,\mathrm{max}}$. The initial opening

[1] The range $i \in [i_{\mathrm{min}}; i_{\mathrm{max}}] \subset [0\,^\circ; 90\,^\circ]$ is chosen just for simplicity – the relation (2.32) is symmetric for inclinations from the range $i \in [0\,^\circ; 90\,^\circ]$ and $i' = 180\,^\circ - i$.

angle $\Delta_{(0)}$ of the Cone reads

$$\begin{aligned} \cos\Delta_{(0)} &\equiv \mathbf{L}_{(0)[1]} \cdot \mathbf{L}_{(0)[6]} \\ &= \cos\left(i_{[6]}\right)\cos\left(i_{[1]}\right) + \sin\left(i_{[6]}\right)\left(i_{[1]}\right)\cos\left[\delta\Omega_{(0)}\right], \quad (3.3) \\ \text{where } \delta\Omega_{(0)} &\equiv \Omega_{(0)[6]} - \Omega_{(0)[1]}, \quad (3.4) \\ i_{[1]} &= i_{(0)[1]} = i_{(t)[1]} = i_{\max}, \quad (3.5) \\ i_{[6]} &= i_{(0)[6]} = i_{(t)[6]} = i_{\min}, \quad (3.6) \end{aligned}$$

and the subscript $_{(t)}$ denotes the time dependence, i.e. $_{(0)} \equiv {}_{(t=0)}$. Let us formulate the criterion of the disk deformation in terms of the Cone opening angle $\Delta_{(t)}$ at an arbitrary time $t > 0$:

> **Criterion 2.** *The stellar disk has lost its initial planar structure, i.e. is deformed, if the Cone opening angle $\Delta_{(t)}$ is larger than a critical value Δ_{crit}.*

The opening angle $\Delta_{(t)}$ expressed in terms of the two "furthest" angular momentum vectors reads:

$$\begin{aligned} \cos\Delta_{(t)} &\equiv \mathbf{L}_{(t)[1]} \cdot \mathbf{L}_{(t)[6]} \\ &= \cos\left(i_{[6]}\right)\cos\left(i_{[1]}\right) + \sin\left(i_{[6]}\right)\sin\left(i_{[1]}\right)\cos\left[\delta\Omega_{(t)}\right], \quad (3.7) \\ &\text{where} \\ \delta\Omega_{(t)} &\equiv \Omega_{(t)[6]} - \Omega_{(t)[1]} \\ &= \delta\Omega_{(0)} - t\,(\mathrm{G}M_\bullet)^{+1/2}\left(\frac{M_{\text{CND}}}{M_\bullet}\right)^{+1} R_{\text{CND}}^{-3}\frac{1+\frac{3}{2}e^2}{\sqrt{1-e^2}} \times \\ &\quad \times \left[a_{[6]}^{+3/2}\cos(i_{[6]}) - a_{[1]}^{+3/2}\cos(i_{[1]})\right] \quad (3.8) \end{aligned}$$

Let us explore the Cone in a given model of the Galactic Centre. Assume that the innermost particle has the inclination $i_{[1]} = 90\,^\circ$. According to formula (2.32), $\Omega_{[1]}$ of this particle is constant, thus angular momentum vector $\mathbf{L}_{[1]}$ of such particle is a constant vector. Therefore, the size of the Cone opening angle depends on the direction of the angular momentum vector $\mathbf{L}_{(t)[6]}$ of the outermost particle. In Fig. 3.1 we show the contour $\Delta_{\text{crit}} = 14\,^\circ$ of the surface $\Delta_{(6\text{ Myr})}(\cos(i_{[6]}), M_{\text{CND}})$. For the outermost test particle moving in the given model of the Galactic Centre (given M_{CND} and the other parameters describing the potential (2.1)) this $\Delta_{(6\text{ Myr})} = \Delta_{\text{crit}}$ contour intersects in a single point $[\cos(i_{[6]}); M_{\text{CND}}; \Delta_{\text{crit}}]$. Since we expect the outermost particle to have the minimal inclination $i_{\min}$ in the sense that $|\cos(i_{\min})|$ is minimal in the ensemble of the test particles,

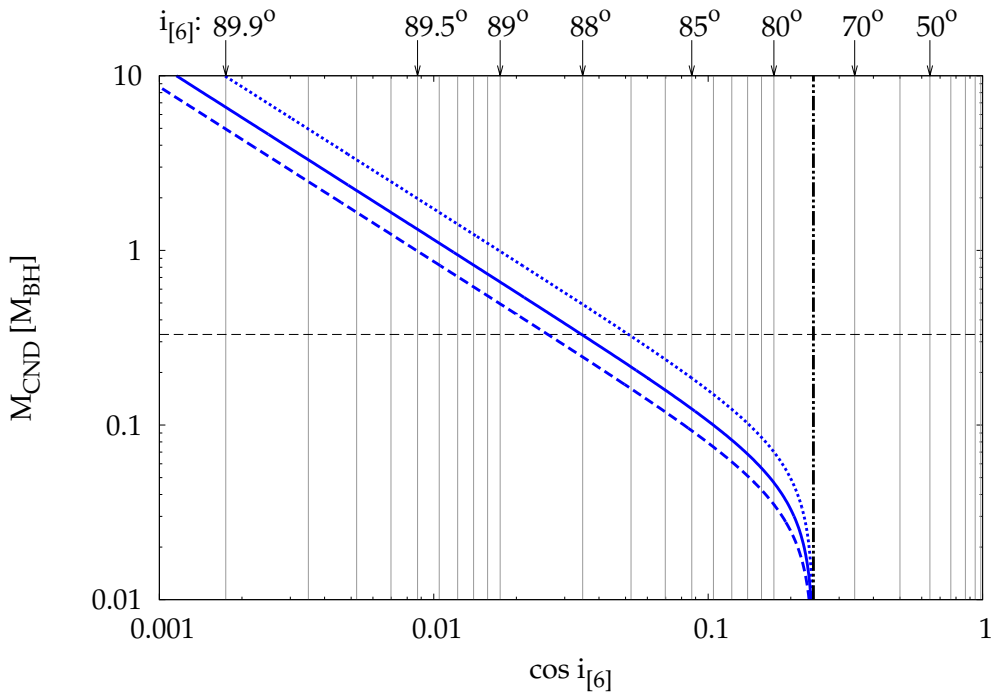

Figure 3.1: Constraints on the initial inclination range by virtue of the Cone critical opening angle $\Delta_{(6\ \mathrm{Myr})[6]} = 14\,^{\circ}$, denoted by the thick curved lines for different ages of the stellar disk population: 4 Myr (dots), 6 Myr (solid curve) and 8 Myr (dashed curve). The horizontal dashed line denotes the current mass estimate $M_{\mathrm{CND}} = \frac{1}{3}\,M_{\bullet}$ by Christopher et al., 2005. The thick vertical line limits the minimal inclination of $76\,^{\circ}$, which represents the minimal inclination limit for $M_{\mathrm{CND}} = 0$. The current M_{CND} estimate implies that the initial inclination range of the clockwise stellar disk could not be broader than $\approx 2\,^{\circ}$ for the stellar age of 6 Myr.

the choice of $\Delta_{\rm crit}$ constraints the range of the initial inclinations. The intersection point of contour $\Delta_{(6\ {\rm Myr})} = \Delta_{\rm crit}$ with given $M_{\rm CND}$ line tells us what the characteristic range of initial inclinations should be so that the Cone opening angle is $\Delta_{\rm crit}$ or smaller. For $M_{\rm CND}/M_\bullet = \frac{1}{3}$, $\Delta_{\rm crit} = 14\,^\circ$ and stellar age 6 Myr the characteristic width of the inclination range cannot exceed $2\,^\circ$. Variation of the stellar age within the range (6 ± 2) Myr results in the characteristic width of the inclination range in $[1.5\,^\circ; 3\,^\circ]$.

On the other hand, fixation of the characteristic width of initial inclination range $\approx 2\,^\circ$ and variation of the Galactic Centre model (variation of $M_{\rm CND}$) tell us that for the stellar age within (6 ± 2) Myr the mass of the circum-nuclear disk should be $M_{\rm CND} \in [0.25; 0.4]\, M_\bullet$. This finding shows that the NIR observations of the positions, proper motions and radial velocities of young stars in the Galactic Centre are in a perfect agreement with the radioastronomical determination of the mass of the circum-nuclear disk.

The choice of $\Delta_{\rm crit}$ plays a role of a free parameter in the evaluation of the disk deformation. Paumard et al., 2006 analysed positions, proper motions and radial velocities of several stars of the clockwise stellar disk and affirmed that this stellar disk has an opening angle $\approx 14\,^\circ$. They confirmed the values of the opening angle proposed by Genzel et al., 2003, Levin & Beloborodov, 2003 and Beloborodov et al., 2006.

We plot three examples of the Cone in Fig. 3.2. The Cone is visualised as the Aitoff projection of a set of angular momentum vectors on a sphere in the $(i;\ \Omega)$ grid. We assume that the stellar disk is a stable structure for 6 Myr and that initially inclinations and semi-major axes were distributed uniformly and $\Omega_{(0)} = 0\,^\circ$ for all particles. According to the findings about the i and Ω temporal evolution, we plot the Cone at the time of 6 Myr afterwards, in order to visually compare its opening angle for different initial inclination ranges.

Let us compare the deformation of the stellar disk according to the Criterion 1 and to the Criterion 2. In Fig. 3.3 we show the contours $\Delta_{(6\ {\rm Myr})} = \Delta_{\rm crit}$ for several $\Delta_{\rm crit} \in [0.125\,^\circ; 90\,^\circ]$ and the contour $\Delta\Omega_{(6\ {\rm Myr})[6]} = 16\,^\circ$. Let us focus on a given Galactic Centre model with $M_{\rm CND} = \frac{1}{3}\, M_\bullet$ and the stellar age 6 Myr. For $\Delta\Omega_{\rm crit} = 16\,^\circ$ Criterion 1 tells us that the stellar disk is deformed if the characteristic width of the initial inclination range is larger than $\approx 3\,^\circ$. On the other hand, for $\Delta_{(6\ {\rm Myr})} = 16\,^\circ$ Criterion 2 tells us that the disk is deformed if the characteristic width of the initial inclination range is larger than $\approx 2\,^\circ$. However, the difference of the single degree does not play an important role in observations, since the angle between the normal vectors to the CND and to the stellar disk cannot be

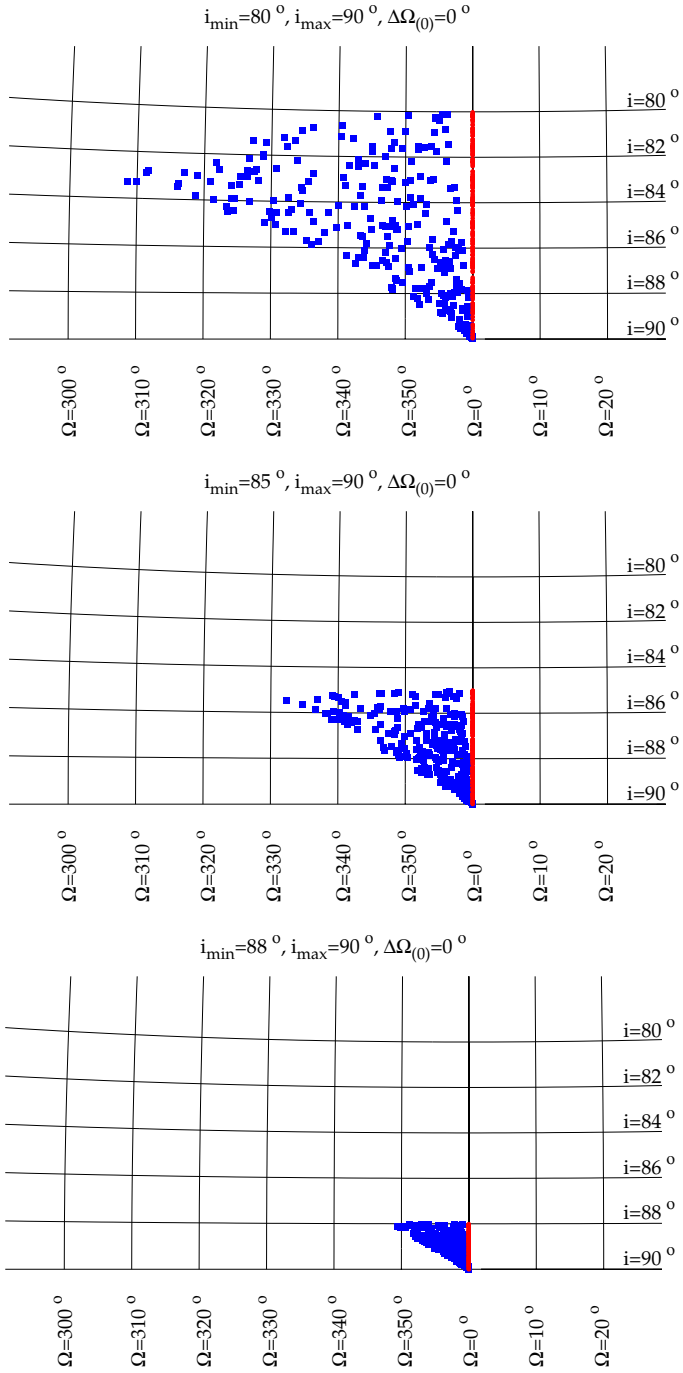

Figure 3.2: Aitoff projection of the Cone in the $(i;\ \Omega)$ grid. The chosen model of the Galactic Centre consists of a super-massive black hole $M_\bullet = 3.5 \times 10^6 M_\odot$, $M_{\rm sphe} = M_\bullet$, $\alpha = 1.75$, $M_{\rm CND} = \frac{1}{3} M_\bullet$ and $R_{\rm CND} = 1.8$ pc. The stellar disk ensemble consists of 250 particles with a uniform distribution of semi-major axes $a \in [0.04; 0.24]$ pc and a uniform distribution of initial inclinations $i_0 \in [i_{\rm min}; 90\,^\circ]$ for $i_{\rm min} = 80\,^\circ$, $85\,^\circ$ and $88\,^\circ$.

determined with such an accuracy nowadays.

In conclusion, the assumption of stability of the stellar disk over the timespan of the stellar age, the observational evidence that the stellar disk is almost perpendicular to the circum-nuclear disk and the choice of $\Delta_{\mathrm{crit}} = 14\,^{\circ}$ tells us that the initial structure was well defined as a planar structure with an opening angle $\lesssim 2\,^{\circ}$. This finding suggests that the stellar disk formed rather via fragmentation of an accretion disk than by an infall of a stellar cluster.

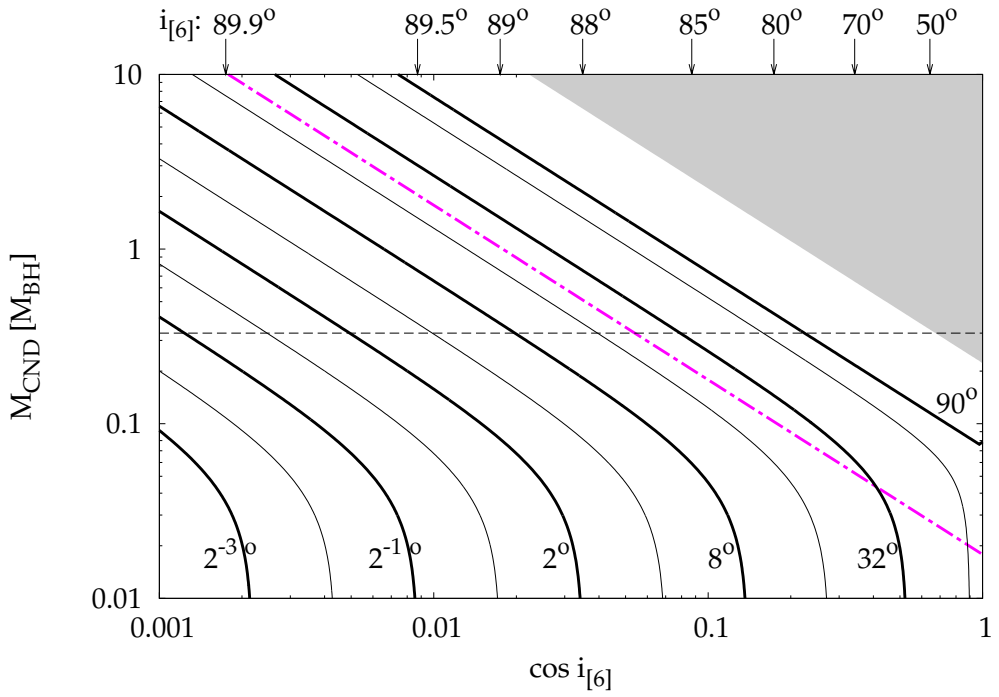

Figure 3.3: Contours of the surface $\Delta_{(6\ \mathrm{Myr})}(\cos(i_{[6]}), M_{\mathrm{CND}})$ for $i_{[1]} = 90\,^{\circ}$. Solid line contours are labelled by the value of $\Delta_{(6\ \mathrm{Myr})}$ in degrees. The diagonal dash-dot line represents the contour $\Omega(\cos(i_{[6]}), M_{\mathrm{CND}}) = 16\,^{\circ}$. The current mass-estimate by Christopher et al., 2005 is denoted by dashed horizontal line. The shaded area represents region where the Criterion 1 is never fulfilled ($\Delta\Omega_{(6\ \mathrm{Myr})[6]} > \Delta\Omega_{\mathrm{max}}$). Chosen $\Delta_{(6\ \mathrm{Myr})}(\cos(i_{[6]}), M_{\mathrm{CND}}) = \Delta_{\mathrm{crit}} < 90\,^{\circ}$, the contour intersects with chosen M_{CND} line at most in 1 point, which denotes i_{min} for the Galactic Centre model. If the particles of the stellar disk have inclinations from the range $i_0 \in [i_{\mathrm{min}}; i_{\mathrm{max}}]$, then according to the Criterion 2, the disk has preserved its initial disk-like structure. If $i_{[6]} \in [0; i_{\mathrm{min}})$ for given M_{CND} and $\Delta_{(6\ \mathrm{Myr})}$, the disk loses its disk-like structure, according to the Criterion 2.

3.2 Cone of angular momentum vectors at $a_{[6]}$

In this section we discuss the opening angle of the cone of angular momentum vectors – hereafter the Cone$_{[6]}$ – of particles from the outer margin of the stellar disk, particles which have $a_{[6]} \equiv a = 0.24$ pc $= 6''$, and the connection of the Cone$_{[6]}$ opening angle to the Cone opening angle.

In the previous Section we discussed the deformation of the whole stellar disk in terms of the Cone of angular momentum vectors of all particles from the stellar disk. As we have shown, the deformation of the disk at a time $t > 0$ depends on the initial configuration of the stellar disk. If the initial configuration of the stellar disk is such that the innermost particles, those with $a_{[1]}$, have an inclination very close to $i = 90\,^\circ$, their angular momentum vectors will remain (almost) constant vectors for all times. Thus, the deformation of the whole stellar disk is then given by the change of $L_{[6]}$ direction from its initial position. Let us consider the relation between the deformation of the whole disk and the deformation of the outer margin of the disk and let us ask, whether Criterion 2 was convenient for the description of the deformation of the stellar disk or not. Let us define the angle $\delta_{(t)}$ between the two "furthest" particles at $a_{[6]}$, i.e. two particles with marginal inclinations of the inclination range, in a similar way as the angle $\Delta_{(t)}$ for the whole disk:

$$\begin{aligned}
\cos\delta_{(t)} &\equiv \mathbf{L}_{(t)[6],\,i_{\min}} \cdot \mathbf{L}_{(t)[6],\,i_{\max}} \\
&= \cos\left(i_{[6],\min}\right)\cos\left(i_{[6],\max}\right) + \sin\left(i_{[6],\min}\right)\sin\left(i_{[6],\max}\right) \times \\
&\quad \times \cos\left\{\delta\Omega_{(0)[6]} - t\,(\mathbb{G}M_\bullet)^{+1/2}\left(\frac{M_{\mathrm{CND}}}{M_\bullet}\right)^{+1} R_{\mathrm{CND}}^{-3}\, a_{[6]}^{+3/2} \times \right. \\
&\quad \left. \times \frac{1+\frac{3}{2}e^2}{\sqrt{1-e^2}}\left[\cos(i_{[6],\max}) - \cos(i_{[6],\min})\right]\right\} \qquad (3.9)
\end{aligned}$$

Let us ask a question, what the initial inclination range of the particles with $a_{[6]}$ should be, so that the outer margin of the inner part of the disk is warped? For this purpose we formulate the third Criterion:

> **Criterion 3.** *The outer margin of the stellar disk is warped, if the Cone$_{[6]}$ opening angle $\delta_{(t)}$ is larger than a critical value δ_{crit}.*

To answer the question, we must consider the choice of δ_{crit} value. According to the current NIR observations of young stars in the clockwise stellar disk, we use $\delta_{\mathrm{crit}} = 14\,^\circ$. Consider the Cone$_{[6]}$ with two "furthest" particles. Assume that particle 1 has the maximal inclination $i_{\max}$ of the $a_{[6]}$

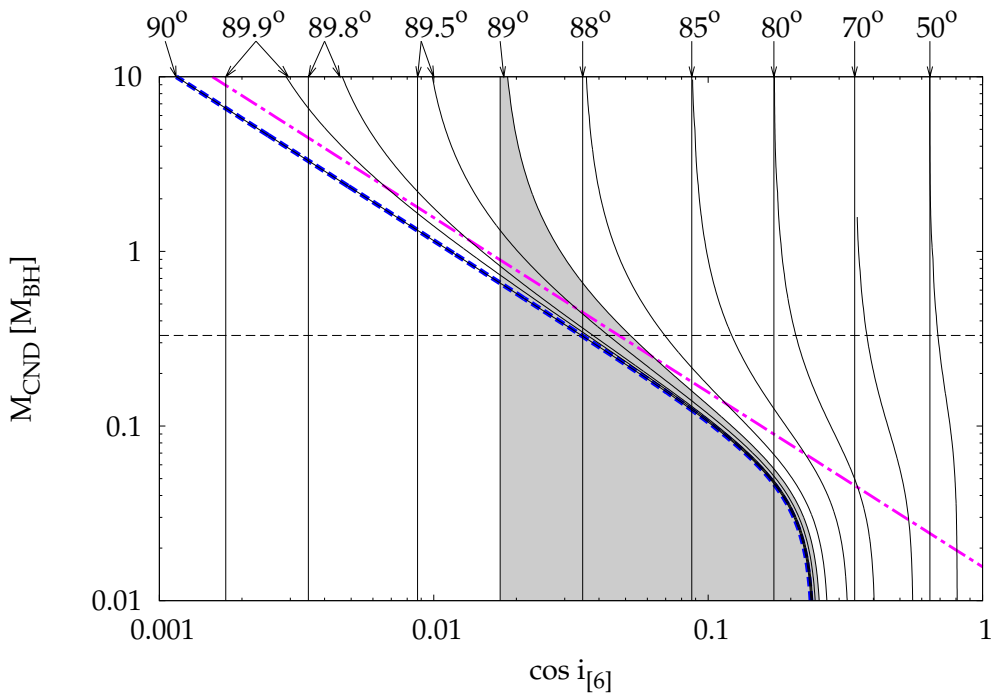

Figure 3.4: Contours of $\delta_{(6\ \mathrm{Myr})}(\cos(i_{\min}), M_{\mathrm{CND}}) = 14^\circ$. Choice of $i_{\max}$ determines the $i_{\min}$ due to (3.9). Every vertical $i_{\max}$ line has its corresponding $i_{\min}$-curve counterpart, the region between the line and the curve has a "drop" like shape. The thick dashed line figures $\Delta_{(6\ \mathrm{Myr})} = 14^\circ$ curve. Note that for $i_{\max} = 90^\circ$ the $\Delta_{(6\ \mathrm{Myr})} = 14^\circ$ and $\delta_{(6\ \mathrm{Myr})} = 14^\circ$ curves are identical, i.e. both Criterions give the same results for the determination of the stellar disk deformation. The shaded area emphasizes the "drop" with $i_{\max} = 89^\circ$. Thick diagonal dash-dot line denotes $\Omega_{(6\ \mathrm{Myr})[6]} - \Omega_{(0)[6]} = 14^\circ$.

ensemble and the particle 2 has the minimal inclination $i_{\min}$. Criterion 3 and equation (3.9) tells us that the outer margin of the inner part of the stellar disk is warped at a time $t > 0$, if $\delta_{(t)} > \delta_{\text{crit}}$. In Fig. 3.4 we show the regions of the initial configuration of a few pairs of the "furthest" $a_{[6]}$ particles. By choosing $i_{\max}$ denoted at the top of Figure, we see what is the possible $i_{\min}$, such that for the given Galactic Centre model (given M_{CND}) the outer margin is not warped at a time $t > 0$ yet. The region inside the $i_{\max}$ and $i_{\min}$ lines fulfils the condition $\delta_{(t)} < \delta_{\text{crit}}$. In Fig. 3.4 we assume the stellar age of 6 Myr. Nevertheless, a variation of the age within the range (6 ± 2) Myr would cause a vertical shift of the "drop" region. Variation of the δ_{crit} choice causes a widening of the "drop" region – the minimal inclination shifts towards lower values (higher $\cos(i_{\min})$ values) for $\delta_{\text{crit}} > 14\,^\circ$, and narrowing of the "drop" for $\delta_{\text{crit}} < 14\,^\circ$. The $i_{\max}$ border would remain preserved.

Let us discuss the deformation of the stellar disk according to Criterion 2 and Criterion 3 at the same time, let $\Delta_{\text{crit}} = \delta_{\text{crit}} = 14\,^\circ$ and the stellar age be 6 Myr. For a fixed model of the Galactic Centre, $M_{\text{CND}} = \frac{1}{3} M_\bullet$, Criterion 2 tells us that the whole disk is not deformed ($\Delta_{(6\text{ Myr})} \leq 14\,^\circ$) for every $i_0 \in [88\,^\circ; 90\,^\circ]$. If $i_{\max} = 90\,^\circ$, Criterion 3 tells us that if the inclination range for the $a_{[6]}$ particle is the same, $i_{[6]} \in [88\,^\circ; 90\,^\circ]$, the outer margin is now warped. If $i_{\max} < 90\,^\circ$, we can find the minimal inclinations, which suggest that despite the fact that the outer margin is not warped ($\delta_{(t)} < \delta_{\text{crit}}$), the whole disk has already lost its disk-like structure ($\Delta_{(t)} > \Delta_{\text{crit}}$).

In conclusion, the choice of Criterion for the evaluation of the disk deformation influences the mass ranges of M_{CND} and the initial inclinations of the disk stars we estimate. Since we are interested in the deformation of the whole stellar disk, we find Criterion 2 more convenient for the determination of the initial inclination range than Criterion 3 in a given Galactic Centre model.

3.3 Angular momentum projected to the direction of line-of-sight

In this section we discuss the evaluation of the disk deformation in terms of the angular momentum projected to the direction of the line-of-sight. Genzel et al., 2003 defined a normalised angular momentum with respect

to the line of sight as

$$j \equiv \frac{J_z}{J_{z,\,\max}} = \frac{xv_y - yv_x}{\sqrt{(x^2+y^2)\left(v_x^2+v_y^2\right)}}. \tag{3.10}$$

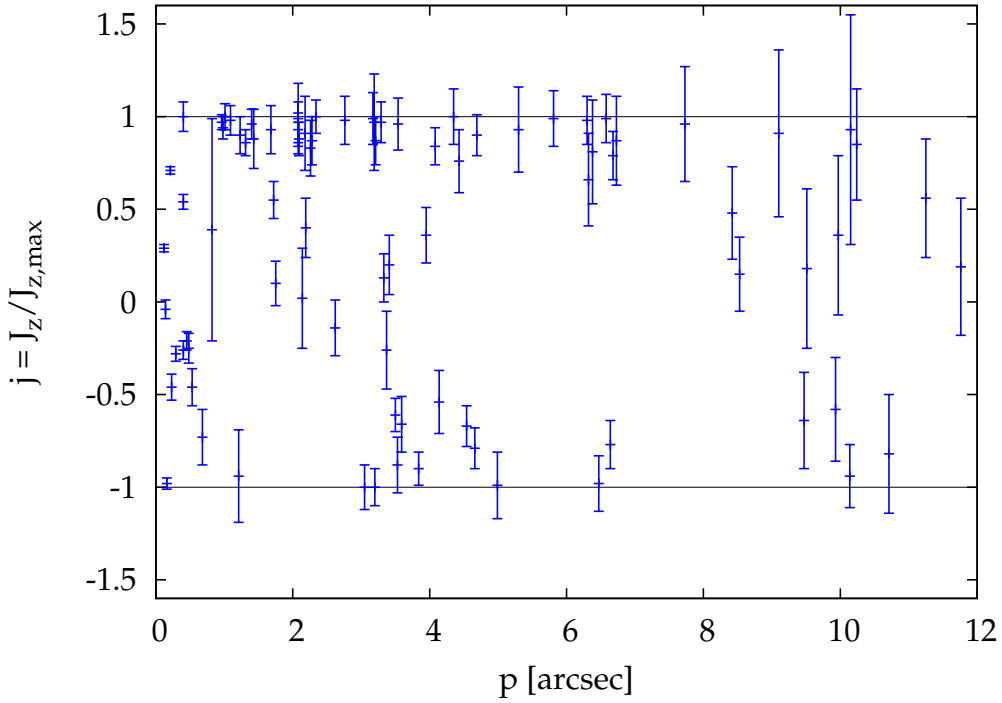

Figure 3.5: Distribution of the projected and normalized angular momentum on the sky $j = J_z/J_{z,\max}$ (3.10) for the early-type stars as a function of the projected separation p from Sgr A* (for $p > 0.08''$). In this diagram stars on projected tangential, clockwise orbits are at $j \simeq +1$, while stars on the tangential, counter-clockwise orbits are at $j \simeq -1$. Stars at $j \simeq 0$ are on projected radial orbits.

They used this quantity as a way to distinguish stars on projected clockwise orbits ($j \simeq +1$) from those on projected counter-clockwise orbits ($j \simeq -1$). This quantity is also a good tool for discrimination between the projected tangential ($|j| \simeq 1$) and the projected radial ($|j| = 0$) orbits.

However, we show that this quantity is an ambiguous and useless tool for the evaluation of the disk deformation from the observed data. We reproduce Fig. 3 from Paumard et al., 2006 in our Fig. 3.5, which shows the normalised angular momentum along the line-of-sight as a function of the

projected radial separation $p = \sqrt{x^2 + y^2}$ from Sgr A* . Let us investigate properties of the projected and normalised angular momentum j as a function of the angle between the direction of line-of-sight and the direction of the normal vector to the stellar disk in case of a test particle moving in a pure Keplerian potential. In the frame corotating with the particle we can describe the position $\mathbf{q}$ and velocity $\dot{\mathbf{q}}$ of the particle with a set of orbital elements as follows:

$$\mathbf{q} = \left[a(\cos E - e);\, a\sqrt{1-e^2}\, \sin E;\, 0 \right], \tag{3.11}$$

$$\dot{\mathbf{q}} = \left[-\frac{na \sin E}{1 - e\cos E};\, \frac{na\sqrt{1-e^2}\cos E}{1 - e\cos E};\, 0 \right], \tag{3.12}$$

where a is the semi-major axis, e eccentricity, E the mean anomaly and n is the mean motion

$$n = \sqrt{\frac{\mathbb{G}M_\bullet}{a^3}} \tag{3.13}$$

Let us define a coordinate frame in the way that its equatorial plane is identical with the plane of the sky and the z axis of this frame is parallel to the direction of the line-of-sight. Then the positions $\mathbf{r}$ and velocities $\dot{\mathbf{r}}$ of a test particle expressed in this frame read

$$\mathbf{r} = R_{xq} \cdot \mathbf{q} = [x; y; z], \tag{3.14}$$

$$\dot{\mathbf{r}} = R_{xq} \cdot \dot{\mathbf{q}} = [v_x; v_y; v_z], \tag{3.15}$$

where the matrix of transformation reads

$$R_{xq} = \begin{bmatrix} \cos(\Omega)\cos(\omega) - \sin(\Omega)\cos(i)\sin(\omega) & -\cos(\Omega)\sin(\omega) - \sin(\Omega)\cos(i)\cos(\omega) & \sin(\Omega)\sin(i) \\ \sin(\Omega)\cos(\omega) + \cos(\Omega)\cos(i)\sin(\omega) & -\sin(\Omega)\sin(\omega) + \cos(\Omega)\cos(i)\cos(\omega) & -\cos(\Omega)\sin(i) \\ \sin(i)\sin(\omega) & \sin(i)\cos(\omega) & \cos(i) \end{bmatrix} \tag{3.16}$$

From (3.10) with the use of (3.14) and (3.15) it follows that j is a function of the angle between the direction of the line-of-sight and the direction of the normal vector to the stellar disk, which we denote i here. In conclusion, j depends on (a, e, i, ω, E), but j does not depend on Ω at all.

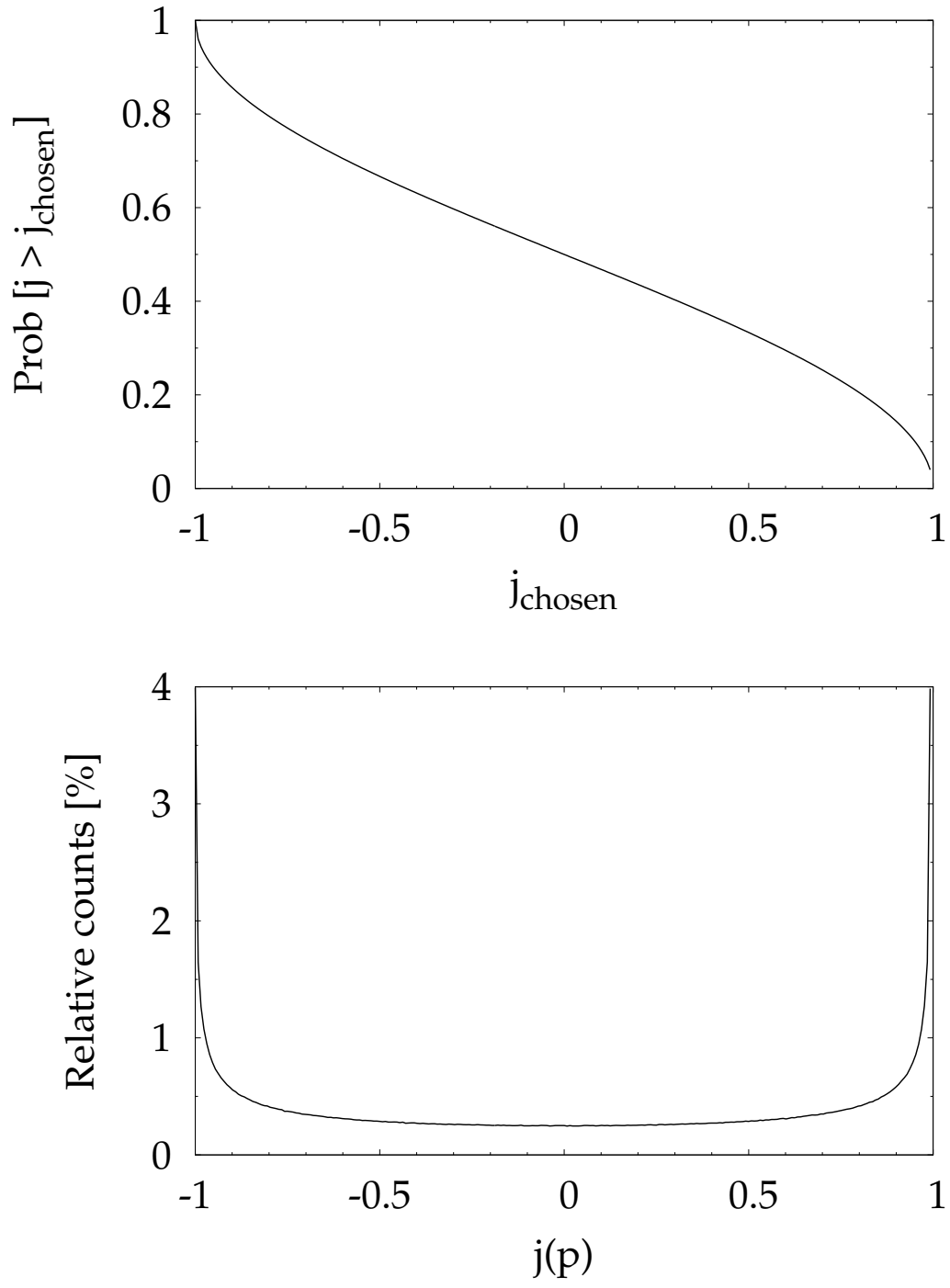

Figure 3.6: Normalised angular momentum of an isotropic stellar cluster. *Top panel:* Cumulative probability that $j(p)$ of a chosen star is larger than a characteristic (chosen) value. $j(p)$ is uniformly distributed in an isotropic cluster. *Bottom panel:* Histogram of distribution of $j(p)$ in an isotropic stellar cluster.

Paumard et al., 2006 in a figure similar to Fig. 3.5 show what is the $j(p)$ distribution for the clockwise disk stars. The stars from the inner part of the clockwise stellar disk, i.e. stars within $a \lesssim 6'' = 0.24$ pc have j close to $+1$ (within errorbars), while the stars from the outer part of the disk, with $a \gtrsim 6''$ reveal a deflection from $j \sim +1$ to radial orbits ($j \sim 0$). This deflection can be a sign of a disk deformation, but the errorbars of the measurements of stars in this region are much larger than those from the inner part. Let us further discuss how the stellar disk deformation influences the $j(p)$ diagram.

Firstly, let us discuss what the $j(p)$ looks like in the case of an isotropic stellar cluster. We have set up a cluster of test particles in an external Keplerian potential with an isotropic spatial distribution, and velocities which correspond to a Keplerian orbit at given position. In Fig. 3.6 we show what the histogram of $j(p)$ for such a cluster looks like. Despite the fact that an isotropic cluster has the most of stars on tangential orbits, either clockwise ($j \simeq +1$) or counter-clockwise ($j \simeq -1$), the cumulative probability that a chosen star from the ensemble has $j(p)$ larger than some characteristic value is approximatively linearly decreasing. Thus, if we have observed an isotropic stellar cluster instead of a stellar disk, we would have seen a uniformly distributed $j(p)$.

Paumard et al., 2006 have determined the eccentrities of the stellar population from the clockwise stellar disk as intermediate ($\lesssim 0.4$). In Fig. 3.7 we show the cumulative probabilities that $j(p)$ is larger than a characteristic value for different small to intermediate eccentrities and different inclinations. According to Paumard et al., 2006 the angle between the normal vector to the clockwise stellar disk and the direction of the line-of-sight is $\approx 53\,^\circ$. However, for inclinations $i \lesssim 50\,^\circ$ and $i \gtrsim 130\,^\circ$ it is quite impossible to determine the inclination from the observational $j(p)$ data. The quantity j would be more helpful, if the clockwise stellar disk was at least $\approx 10\,^\circ$ more side-on. As this is not the case, the normalised angular momentum j projected to direction of the line-of-sight is inconvenient quantity to explore the small deformation ($\Delta_{(6\ \mathrm{Myr})} \approx 10\,^\circ$) $\approx 50\,^\circ$ angle-wise, i.e. for the exploration of the deformation of the clockwise stellar disk.

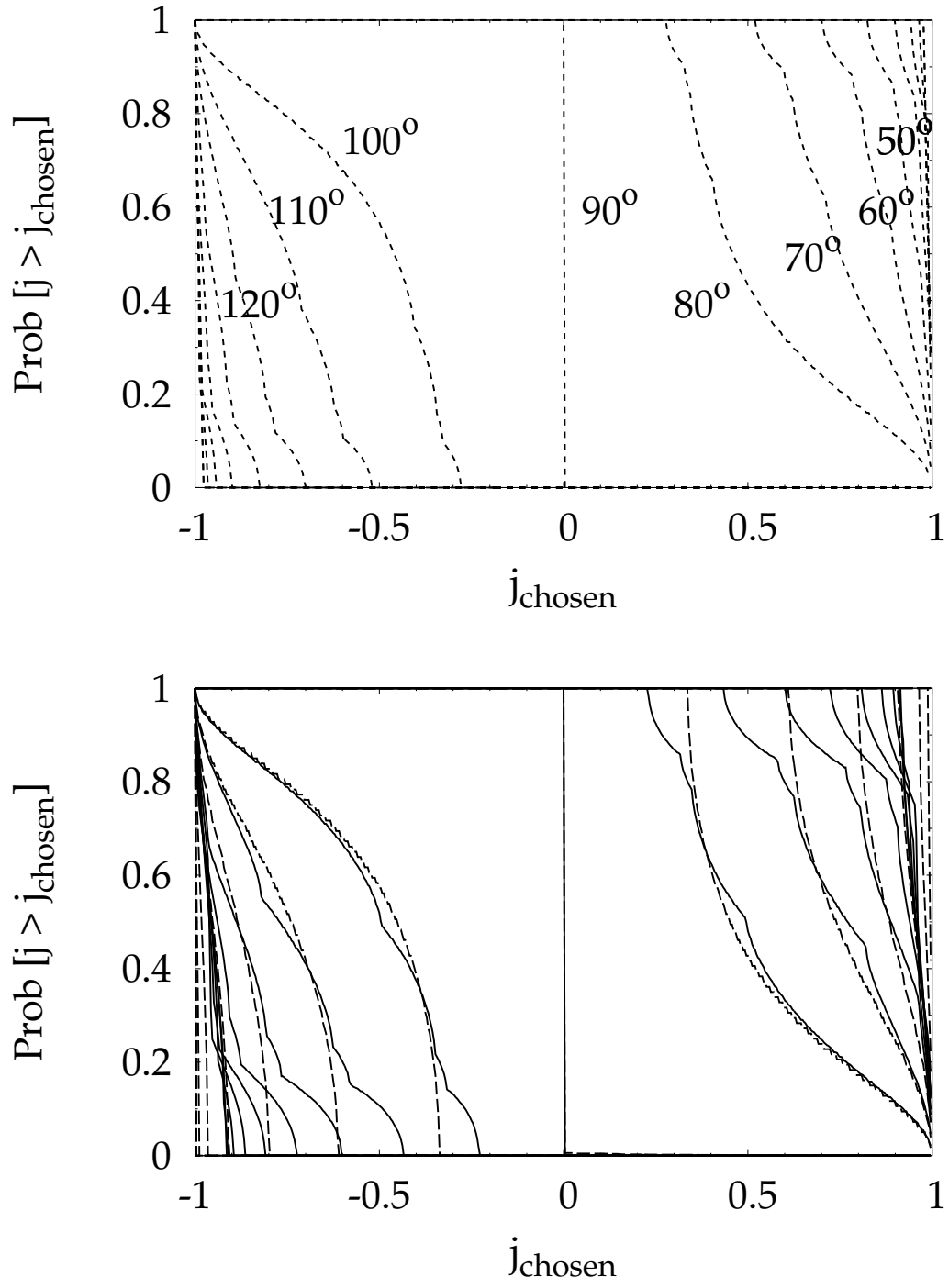

Figure 3.7: Cumulative probability that $j(p) > j_{\rm chosen}$ for different $i \in [0\,^\circ; 180\,^\circ]$ with the step of $10\,^\circ$ (several values of i highlighted) and different e. *Top panel:* Set of test particles with $e = 0.2$. *Bottom panel:* $e = 0$ (dash) and $e = 0.4$ (solid line). Note the over-density of lines for $i \lesssim 50\,^\circ$ and $i \gtrsim 130\,^\circ$.

4 Conclusions

Model We modelled the motion of stars from the clockwise stellar disk in the dominating Keplerian potential of Sgr A* perturbed by the circum-nuclear disk and the spherical cluster of old stars. The stars of the stellar disk were modelled as test particles moving in the composed potential. We assumed the stellar disk is a stable structure in the timespan of 6 Myr.

Results We found that the presence of the spherical stellar cluster with the total mass $M_{\mathrm{sphe}}/M_{\mathrm{CND}} \gtrsim 1/20$ increases the frequencies and damps the amplitudes of the oscillations of the eccentricity e and the inclination i due to the apsidal precession ω. Fast changes of ω affect temporal evolution of the longitude of the ascending node Ω, which then precedes linearly with time.

We have explored the timescale of the Ω changes and its dependence on a set of parameters describing the Galactic Centre model and the orbital elements of a test particle and shown these dependences in equation (2.30). We used these findings about the temporal evolution of the orbital elements in the investigation of the deformation of the stellar disk.

We found that the stellar disk formed almost perpendicular to the circum-nuclear disk. Furthermore, we found out that the stellar disk was indeed a planar structure with the opening angle $\approx 2\,^\circ$. Such an opening angle requires a mass of the circum-nuclear disk in the range $M_{\mathrm{CND}} \in [0.25; 0.4]\, M_\bullet$, which embraces the current observational estimate by Christopher et al., 2005.

Moreover, our model of the Galactic Centre shows that such a high collimation of the planar structure suggests that the stellar disk probably did not form via an infall of a stellar cluster. However, the collimation indicates that formation of the stellar disk via fragmentation of an accretion disk is a plausible scenario.

Limitations We considered all potentials as purely Newtonian. Therefore, the post-Newtonian approach represents a possible improvement on the way to a more realistic description of the Galactic Centre environment. We treated the CND as an infinitely thin ring. Thus, a consideration of

other axially symmetric potentials comes into question.

Since we modelled the stellar disk as a set of test particles, we neglected e.g. mutual interactions among stars. Consequently, our model does not reflect the dynamical evolution of the young stellar cluster due to the two-body relaxation, which could affect the deformation of the stellar disk in the timespan of the relaxation time of the stellar cluster. We also neglected any kind of non-gravitational interactions and the stellar evolution.

Outlook Despite all the simplifications we have made, our model of the Galactic centre shows that the radioastronomical observations and measurements of the circum-nuclear disk mass are in agreement with the diffraction-limited NIR observations of the young stellar disk. Consequently, with an improved observational instrumentation, observers acquire more accurate measurements, which then provide us with better knowledge of the environment required for the design of more precise models.

A The Quadrupole Equations

The quadrupole equations represent an approximative description of the temporal evolution of the orbital elements of a satellite in the hierarchical three-body problem (star-planet-satellite). Here we present a more detailed summary of the derivation of the satellite's equations of motion, which can be assembled from information found in Brouwer & Clemence, 1961 and in Ćuk & Burns, 2004.

In this Thesis we study the motion of a test particle under the influence of axially symmetric and spherical perturbations to the central potential of the super-massive black hole. If the spherical perturbation was sufficiently negligible to the central mass potential, the quadrupole equations would describe the motion of the test particle. The test particle would replace the "satellite" in the following derivation, the axially symmetric perturbation would then represent the "star" in the hierarchical model and the super-massive black hole would then be the "planet". Let us study the motion of a satellite in a hierarchical triple system consisting of a star, a planet orbiting the star, and a satellite orbiting the planet. Let the star (mass $M_\star$) and the planet (mass $M_{\rm pl}$) be considered as point masses and let the mass of the satellite be negligible. Let x, y, z be the coordinates of the satellite and $x_\star$, $y_\star$, $z_\star$ the coordinates of the star in a Cartesian coordinate system with its centre at the planet position. The equations of motion for the satellite are

$$\begin{aligned}
\frac{\mathrm{d}^2x}{\mathrm{d}t^2} + \mathbb{G}M_{\rm pl}\frac{x}{r^3} &= \frac{\partial R}{\partial x},\\
\frac{\mathrm{d}^2y}{\mathrm{d}t^2} + \mathbb{G}M_{\rm pl}\frac{y}{r^3} &= \frac{\partial R}{\partial y},\\
\frac{\mathrm{d}^2z}{\mathrm{d}t^2} + \mathbb{G}M_{\rm pl}\frac{z}{r^3} &= \frac{\partial R}{\partial z},
\end{aligned} \tag{A.1}$$

where $r^2 = x^2 + y^2 + z^2$, and R is the disturbing function describing the influence of the star on the satellite:

$$R = \mathbb{G}M_\star\left(\frac{1}{\Delta} - \frac{xx_\star + yy_\star + zz_\star}{r_\star^3}\right), \tag{A.2}$$

the distance of the star from the satellite Δ is given by

$$\begin{aligned}\Delta^2 &= (x-x_\star)^2+(y-y_\star)^2+z^2\\ &= r_\star^2+r^2-2(xx_\star+yy_\star)\\ &= r_\star^2+r^2-2r_\star r\cos\psi,\end{aligned} \tag{A.3}$$

where ψ is the angle between $\vec{r}_\star$ and $\vec{r}$. The orbit of the planet around the star is considered to be an ellipse in a fixed plane, therefore the coordinate system is chosen such that $z_\star = 0$. From (A.3) it follows that

$$\frac{r_\star}{\Delta} = \left[1+\left(\frac{r}{r_\star}\right)^2-2\frac{r}{r_\star}\cos\psi\right]^{-1/2}. \tag{A.4}$$

If the ratio $\rho = r/r_\star$ is sufficiently small, we can expand $r_\star/\Delta$ in terms of ρ. In order to do so, it is useful to introduce substitution

$$2\cos\psi = \eta+\eta^{-1} \tag{A.5}$$

and rewrite (A.4) in terms of ρ and η:

$$\frac{r_\star}{\Delta} = \left[\left(1-\rho\eta\right)\left(1-\rho\eta^{-1}\right)\right]^{-1/2}. \tag{A.6}$$

The use of the Taylor expansion and grouping together terms with the same power in ρ, and trigonometric relations enable us to rewrite the $r_\star/\Delta$ ratio in terms of the Legendre polynomials with the argument $\cos\psi$:

$$\begin{aligned}\frac{r_\star}{\Delta} &= \left[\left(1-\rho\eta\right)\left(1-\rho\eta^{-1}\right)\right]^{-1/2}\\ &= \left(1+\frac{1}{2}\rho\eta+\frac{3}{8}(\rho\eta)^2+\frac{5}{16}(\rho\eta)^3+\ldots\right)\cdot\\ &\qquad\cdot\left(1+\frac{1}{2}\rho\eta^{-1}+\frac{3}{8}(\rho\eta^{-1})^2+\frac{5}{16}(\rho\eta^{-1})^3+\ldots\right)\\ &= 1+\frac{1}{2}\rho(\eta+\eta^{-1})+\\ &\quad+\rho^2\left[\frac{1}{4}+\frac{3}{8}(\eta^2+\eta^{-2})\right]+\\ &\quad+\rho^3\left[\frac{3}{16}(\eta+\eta^{-1})+\frac{5}{16}(\eta^3+\eta^{-3})\right]+\ldots\\ &= 1+\rho\cos\psi+\rho^2\left[\frac{1}{4}+\frac{3}{4}\cos 2\psi\right]+\rho^3\left[\frac{3}{8}\cos\psi+\frac{5}{8}\cos 3\psi\right]+\ldots\\ &= 1+\rho\cos\psi+\rho^2\left[-\frac{1}{2}+\frac{3}{2}\cos^2\psi\right]+\rho^3\left[-\frac{3}{2}\cos\psi+\frac{5}{2}\cos^3\psi\right]+\ldots\\ \frac{r_\star}{\Delta} &= 1+\rho P_1(\cos\psi)+\rho^2P_2(\cos\psi)+\rho^3P_3(\cos\psi)+\ldots\end{aligned} \tag{A.7}$$

Since

$$\frac{xx_\star + yy_\star}{r_\star^3} = \frac{r\cos\psi}{r_\star^2} = \rho\frac{\cos\psi}{r_\star} \quad \text{and} \quad z_\star = 0,$$

the disturbing function R can be written as

$$\begin{aligned} R &= \frac{\mathbb{G}M_\star}{r_\star}\frac{r_\star}{\Delta} - \mathbb{G}M_\star\frac{xx_\star + yy_\star}{r_\star^3} - \mathbb{G}M_\star\frac{zz_\star}{r_\star^3} \\ &= \frac{\mathbb{G}M_\star}{r_\star}\left[1 + \rho P_1(\cos\psi) + \rho^2 P_2(\cos\psi) + \rho^3 P_3(\cos\psi) + \ldots\right] - \frac{\mathbb{G}M_\star}{r_\star}\rho\cos\psi \\ &= \frac{\mathbb{G}M_\star}{r_\star}\left[1 + \rho^2\left(-\frac{1}{2} + \frac{3}{2}\cos^2\psi\right) + \rho^3\left(-\frac{3}{2} + \frac{5}{2}\cos^3\psi\right) + \ldots\right]. \end{aligned}$$

Finally, the term $\mathbb{G}M_\star/r_\star$ does not depend on satellite's coordinates, therefore it will not contribute to the right-hand sides of (A.1) and it is possible to write the disturbing function R as follows:

$$R = \frac{\mathbb{G}M_\star}{r_\star}\left[\left(\frac{r}{r_\star}\right)^2\left(-\frac{1}{2} + \frac{3}{2}\cos^2\psi\right) + \left(\frac{r}{r_\star}\right)^3\left(-\frac{3}{2} + \frac{5}{2}\cos^3\psi\right) + \ldots\right].$$

Hence, the quadrupole approximation to the disturbing function R_q reads

$$R_\mathrm{q} = \mathbb{G}M_\star\frac{r^2}{2r_\star^3}\left(3\cos^2\psi - 1\right). \tag{A.8}$$

Spherical trigonometry provides us with expansion of $\cos\psi$:

$$\cos\psi = \cos(\omega_\star + v_\star)\cos(\omega + v) + \sin(\omega_\star + v_\star)\sin(\omega + v)\cos i,$$

where $\omega_\star$ is the argument of periapsis, $v_\star$ is the true anomaly of the star, ω is the argument of periapsis, v is the true anomaly and i is the inclination of the satellite's orbit to the planet's orbital plane. Thus, the quadrupole disturbing function R_q can be written as

$$R_\mathrm{q} = \frac{\mathbb{G}M_\star}{2r_\star^3}\left(3R_{\mathrm{q},1} + 3R_{\mathrm{q},2} + 6R_{\mathrm{q},12}\cos i - R_{\mathrm{q},0}\right), \tag{A.9}$$

where

$$\begin{aligned} R_{\mathrm{q},1} &= r^2\cos^2(\omega_\star + v_\star)\left[\cos^2(\omega)\cos^2(v) - \right. \\ &\qquad \left. -\frac{1}{2}\sin(2\omega)\sin(2v) + \sin^2(\omega)\sin^2(v)\right], \qquad \text{(A.10)} \\ R_{\mathrm{q},2} &= r^2\sin^2(\omega_\star + v_\star)\left[\cos^2(\omega)\sin^2(v) + \right. \\ &\qquad \left. +\frac{1}{2}\sin(2\omega)\sin(2v) + \sin^2(\omega)\cos^2(v)\right], \qquad \text{(A.11)} \end{aligned}$$

$$\begin{aligned} R_{\mathrm{q},12} &= \frac{1}{4} r^2 \sin[2(\omega_\star + v_\star)] \left[\cos(2\omega)\sin(2v) + \right. \\ &\qquad \left. + \sin(2\omega)\cos(2v)\right], \qquad \text{(A.12)} \\ R_{\mathrm{q},0} &= r^2. \qquad \text{(A.13)} \end{aligned}$$

In the equations (A.10)-(A.13) the dependence on ω and v is separated in order to prepare the disturbing function for averaging over the satellite's orbital motion. We average R_q over v by integration

$$\langle R_{\mathrm{q},i} \rangle = \frac{1}{2\pi} \int_0^{2\pi} R_{\mathrm{q},i} n \, \mathrm{d}t. \qquad \text{(A.14)}$$

The easiest way to perform such integration is by expressing r, v and $n\,\mathrm{d}t$ in terms of the eccentric anomaly E:

$$\begin{aligned} r &= a[1 - e\cos(E)], \qquad \text{(A.15)} \\ \cos(v) &= \frac{\cos(E) - e}{1 - e\cos(E)}, \qquad \text{(A.16)} \\ \sin(v) &= \frac{\sqrt{1-e^2}\sin(E)}{1 - e\cos(E)}, \qquad \text{(A.17)} \\ \tan\left(\frac{v}{2}\right) &= \sqrt{\frac{1+e}{1-e}} \tan\left(\frac{E}{2}\right), \qquad \text{(A.18)} \\ n\,\mathrm{d}t &= [1 - e\cos(E)]\ \mathrm{d}E. \qquad \text{(A.19)} \end{aligned}$$

During the averaging process we make use of these five terms:

$$\begin{aligned} \langle r^2 \rangle &= \frac{1}{2\pi} \int_0^{2\pi} r^2 n \, \mathrm{d}t \\ &= \frac{1}{2\pi} \int_0^{2\pi} a^2 [1 - e\cos(E)]^3 \ \mathrm{d}E \\ &= a^2 \left(1 + \frac{3}{2} e^2\right), \qquad \text{(A.20)} \\ \langle r^2 \cos^2(v) \rangle &= \frac{1}{2\pi} \int_0^{2\pi} r^2 \cos^2(v) n \, \mathrm{d}t \\ &= \frac{1}{2\pi} \int_0^{2\pi} a^2 [1 - e\cos(E)][\cos(E) - e]^2 \ \mathrm{d}E \\ &= a^2 \left(\frac{1}{2} + 2e^2\right), \qquad \text{(A.21)} \end{aligned}$$

$$\begin{aligned}
\langle r^2 \sin^2(v)\rangle &= \frac{1}{2\pi}\int_0^{2\pi} r^2 \sin^2(v) n \, \mathrm{d}t \\
&= \frac{1}{2\pi}\int_0^{2\pi} a^2[1-e\cos(E)](1-e^2)\sin^2(E) \, \mathrm{d}E \\
&= \frac{1}{2}a^2\left(1-e^2\right), \qquad \text{(A.22)} \\
\langle r^2 \sin(2v)\rangle &= \frac{1}{2\pi}\int_0^{2\pi} r^2 \sin(2v) n \, \mathrm{d}t \\
&= \frac{2a^2}{2\pi}\int_0^{2\pi}\left[\sqrt{1-e^2}\sin(E)\right]\left[\cos(E)-e\right]\cdot \\
&\qquad \cdot\left[1-e\cos(E)\right] \, \mathrm{d}E \\
&= 0, \qquad \text{(A.23)} \\
\langle r^2 \cos(2v)\rangle &= \frac{1}{2\pi}\int_0^{2\pi} r^2 \cos(2v) n \, \mathrm{d}t \\
&= \frac{1}{2\pi}\int_0^{2\pi} r^2\left[\cos^2(v)-\sin^2(v)\right] n \, \mathrm{d}t \\
&= \frac{5}{2}a^2e^2. \qquad \text{(A.24)}
\end{aligned}$$

Averaging the terms (A.10)-(A.13) over the satellite's motion now yields

$$\begin{aligned}
\langle R_{\mathrm{q},1}\rangle &= \cos^2(\omega_\star + v_\star)\left[\cos^2(\omega)\langle r^2\cos^2(v)\rangle - \right. \\
&\quad \left. -\frac{1}{2}\sin(2\omega)\langle r^2\sin(2v)\rangle + \sin^2(\omega)\langle r^2\sin^2(v)\rangle\right] \\
&= a^2\cos^2(\omega_\star+v_\star)\left[\frac{1}{2}(1-e^2)+\frac{5}{2}e^2\cos^2(\omega)\right], \qquad \text{(A.25)} \\
\langle R_{\mathrm{q},2}\rangle &= \sin^2(\omega_\star + v_\star)\left[\cos^2(\omega)\langle r^2\sin^2(v)\rangle + \right. \\
&\quad \left. +\frac{1}{2}\sin(2\omega)\langle r^2\sin(2v)\rangle + \sin^2(\omega)\langle r^2\cos^2(v)\rangle\right] \\
&= a^2\sin^2(\omega_\star+v_\star)\left[\frac{1}{2}(1-e^2)+\frac{5}{2}e^2\sin^2(\omega)\right], \qquad \text{(A.26)} \\
\langle R_{\mathrm{q},12}\rangle &= \frac{1}{4}\sin[2(\omega_\star+v_\star)]\left[\cos(2\omega)\langle r^2\sin(2v)\rangle + \right. \\
&\quad \left. +\sin(2\omega)\langle r^2\cos(2v)\rangle\right] \\
&= \frac{5}{8}a^2\sin[2(\omega_\star+v_\star)]\, e^2\sin(2\omega), \qquad \text{(A.27)}
\end{aligned}$$

$$\langle R_{\mathrm{q},0}\rangle \;=\; \langle r^2\rangle = a^2\left(1+\frac{3}{2}e^2\right). \tag{A.28}$$

Averaging R_{q} over v now involves replacing terms (A.10)-(A.13) with their averaged companions (A.25)-(A.28) in (A.9):

$$\langle R_{\mathrm{q}}\rangle \;=\; \frac{\mathbb{G}M_\star}{2r_\star^3}\left[3\langle R_{\mathrm{q},1}\rangle + 3\langle R_{\mathrm{q},2}\rangle + 6\langle R_{\mathrm{q},12}\rangle\cos i - \langle R_{\mathrm{q},0}\rangle\right]. \tag{A.29}$$

In order to obtain the quadrupole equations the R_{q} term must be averaged over the satellite's motion and over the star's motion. The averaging over v resulted in (A.29). In order to perform the averaging over the motion of the star, we split (A.29) into three parts: the part which does not depend on $2(\omega_\star + v_\star)$, and the part which does depend on $2(\omega_\star + v_\star)$ only, and the part which depends on both $2(\omega)$ and $2(\omega_\star + v_\star)$. Thus,

$$\langle R_{\mathrm{q}}\rangle \;=\; \langle R_{\mathrm{q},A}\rangle + \langle R_{\mathrm{q},B}\rangle + \langle R_{\mathrm{q},C}\rangle, \tag{A.30}$$

where

$$\begin{aligned}
\langle R_{\mathrm{q},A}\rangle \;&=\; \mathbb{G}M_\star\frac{a^2}{2r_\star^3}\left[-\frac{2}{8}-\frac{3}{8}e^2+\frac{15}{8}e^2\cos(2\omega)+\frac{6}{8}\cos^2 i+\right.\\
&\quad\left.+\frac{9}{8}e^2\cos^2 i-\frac{15}{8}e^2\cos^2 i\cos(2\omega)\right], \qquad (A.31)\\
\langle R_{\mathrm{q},B}\rangle \;&=\; \mathbb{G}M_\star\frac{a^2}{2r_\star^3}\left[\frac{6}{8}\cos[2(\omega_\star+v_\star)]+\frac{9}{8}e^2\cos[2(\omega_\star+v_\star)]-\right.\\
&\quad-\frac{6}{8}\cos^2 i\cos[2(\omega_\star+v_\star)]-\\
&\quad\left.-\frac{9}{8}e^2\cos^2 i\cos[2(\omega_\star+v_\star)]\right], \qquad (A.32)\\
\langle R_{\mathrm{q},C}\rangle \;&=\; \mathbb{G}M_\star\frac{a^2}{2r_\star^3}\left[\frac{15}{8}e^2\cos[2(\omega_\star+v_\star)]\cos(2\omega)(1+\cos^2 i)+\right.\\
&\quad\left.+\frac{15}{8}e^2 2\cos i\sin[2(\omega_\star+v_\star)]\sin(2\omega)\right]. \qquad (A.33)
\end{aligned}$$

Now, the averaging of (A.29) over the motion of the star will be carried out through averaging over the star's mean anomaly $m_\star$. This can be done using the following useful relations:

$$\frac{1}{2\pi}\int_0^{2\pi}\left(\frac{a_\star}{r_\star}\right)^3 n_\star\,\mathrm{d}t = \frac{1}{2\pi}\int_0^{2\pi}\left(\frac{a_\star}{r_\star}\right)^3 \mathrm{d}m_\star = (1-e_\star^2)^{-3/2}, \tag{A.34}$$

$$\frac{1}{2\pi}\int_0^{2\pi}\frac{a_\star^3}{r_\star^3}\cos[2(\omega_\star+v_\star)]\,\mathrm{d}m_\star = 0 = \frac{1}{2\pi}\int_0^{2\pi}\frac{a_\star^3}{r_\star^3}\sin[2(\omega_\star+v_\star)]\,\mathrm{d}m_\star. \tag{A.35}$$

The term $\langle R_{\mathrm{q},A}\rangle$ does depend on $v_\star$ only via $r_\star^{-3}$, thus the averaging over the motion of the star will employ formula (A.34):

$$\begin{aligned}\langle\langle R_{\mathrm{q},A}\rangle\rangle_\star &= \frac{1}{2\pi}\int_0^{2\pi}\langle R_{\mathrm{q},A}\rangle\, n_\star\,\mathrm{d}t \\ &= \mathcal{G}M_\star\frac{a^2}{2a_\star^3}\,[\ldots]\,\frac{1}{2\pi}\int_0^{2\pi}\left(\frac{a_\star}{r_\star}\right)^3 n_\star\,\mathrm{d}t,\end{aligned}$$

$$\langle\langle R_{\mathrm{q},A}\rangle\rangle_\star = \frac{\mathcal{G}M_\star a^2}{8a_\star^3(1-e_\star^2)^{3/2}}\left\{2+3e^2-3\sin^2(i)\left[1+e^2(4-5\cos^2(\omega))\right]\right\}. \tag{A.36}$$

Averaging the terms $\langle R_{\mathrm{q},B}\rangle$ and $\langle R_{\mathrm{q},C}\rangle$ over the motion of the star will employ formula (A.35):

$$\begin{aligned}\langle\langle R_{\mathrm{q},B}\rangle\rangle_\star &= \frac{1}{2\pi}\int_0^{2\pi}\langle R_{\mathrm{q},B}\rangle\, n_\star\,\mathrm{d}t \\ &= \mathcal{G}M_\star\frac{a^2}{2a_\star^3}\,[\ldots]\sin^2(i)\,\frac{1}{2\pi}\int_0^{2\pi}\left(\frac{a_\star}{r_\star}\right)^3\cos[2(\omega+v)]\,n_\star\,\mathrm{d}t, \\ \langle\langle R_{\mathrm{q},C}\rangle\rangle_\star &= \frac{1}{2\pi}\int_0^{2\pi}\langle R_{\mathrm{q},C}\rangle\, n_\star\,\mathrm{d}t = \mathcal{G}M_\star\frac{a^2}{2a_\star^3}\frac{15}{8}e^2\times \\ &\quad\times\left[\cos(2\omega)(1+\cos^2 i)\,\frac{1}{2\pi}\int_0^{2\pi}\left(\frac{a_\star}{r_\star}\right)^3\cos[2(\omega_\star+v_\star)]\,n_\star\,\mathrm{d}t+\right. \\ &\quad\left.+2\cos i\sin(2\omega)\,\frac{1}{2\pi}\int_0^{2\pi}\left(\frac{a_\star}{r_\star}\right)^3\sin[2(\omega_\star+v_\star)]\,n_\star\,\mathrm{d}t\right],\end{aligned}$$

$$\langle\langle R_{\mathrm{q},B}\rangle\rangle_\star = 0 = \langle\langle R_{\mathrm{q},C}\rangle\rangle_\star. \tag{A.37}$$

Finally, according to (A.29), (A.36) and (A.37), the quadrupole approximation to the disturbing function averaged over the motion of the satellite and over the motion of the star reads

$$\begin{aligned}\langle\langle R_{\mathrm{q}}\rangle\rangle_\star &= \langle\langle R_{\mathrm{q},A}\rangle\rangle_\star+\langle\langle R_{\mathrm{q},B}\rangle\rangle_\star+\langle\langle R_{\mathrm{q},C}\rangle\rangle_\star \\ &= \frac{\mathcal{G}M_\star a^2}{8a_\star^3(1-e_\star^2)^{3/2}}\left\{2+3e^2-3\sin^2(i)\left[1+e^2(4-5\cos^2(\omega))\right]\right\}.\end{aligned} \tag{A.38}$$

Inserting $R_{\rm AVG} \equiv \langle\langle R_{\rm q}\rangle\rangle_\star$ into the Lagrange planetary equations will give us the quadrupole equations. The Lagrange planetary equations read

$$\frac{{\rm d}a}{{\rm d}t} = \frac{2}{na}\frac{\partial R_{\rm AVG}}{\partial m}, \tag{A.39}$$

$$\frac{{\rm d}e}{{\rm d}t} = \frac{1-e^2}{na^2e}\frac{\partial R_{\rm AVG}}{\partial m} - \frac{\sqrt{(1-e^2)}}{na^2e}\frac{\partial R_{\rm AVG}}{\partial \omega}, \tag{A.40}$$

$$\frac{{\rm d}i}{{\rm d}t} = \frac{\cot{\rm g}\, i}{na^2\sqrt{1-e^2}}\frac{\partial R_{\rm AVG}}{\partial \omega}, \tag{A.41}$$

$$\frac{{\rm d}\omega}{{\rm d}t} = \frac{-\cot{\rm g}\, i}{na^2\sqrt{1-e^2}}\frac{\partial R_{\rm AVG}}{\partial i} + \frac{\sqrt{1-e^2}}{na^2e}\frac{\partial R_{\rm AVG}}{\partial e}, \tag{A.42}$$

$$\frac{{\rm d}\Omega}{{\rm d}t} = \frac{-\csc i}{na^2\sqrt{1-e^2}}\frac{\partial R_{\rm AVG}}{\partial i}, \tag{A.43}$$

$$\frac{{\rm d}m}{{\rm d}t} = n - \frac{1-e^2}{na^2e}\frac{\partial R_{\rm AVG}}{\partial e} - \frac{2}{na}\frac{\partial R_{\rm AVG}}{\partial a}. \tag{A.44}$$

Since we are looking for evolutionary equations for e, i, ω and Ω, it is necessary to evaluate the the partial derivatives of $R_{\rm AVG}$ with respect to e, i, ω and m:

$$\frac{\partial R_{\rm AVG}}{\partial e} = \frac{6\mathbb{G}M_\star e a^2}{8a_\star^3(1-e_\star^2)^{3/2}}\{1-\sin^2(i)[4-5\cos^2(\omega)]\}, \tag{A.45}$$

$$\frac{\partial R_{\rm AVG}}{\partial i} = \frac{-3\mathbb{G}M_\star a^2\sin(2i)}{8a_\star^3(1-e_\star^2)^{3/2}}[1+4e^2-5e^2\cos^2(\omega)], \tag{A.46}$$

$$\frac{\partial R_{\rm AVG}}{\partial \omega} = \frac{-15\mathbb{G}M_\star a^2e^2}{8a_\star^3(1-e_\star^2)^{3/2}}\sin^2(i)\sin(2\omega), \tag{A.47}$$

$$\frac{\partial R_{\rm AVG}}{\partial m} = 0. \tag{A.48}$$

Last, inserting these partial derivatives into the Lagrange planetary equations gives rise to the quadrupole equations:

$$\frac{{\rm d}e}{{\rm d}\tau} = \frac{15}{8}e\sqrt{1-e^2}\sin^2(i)\sin(2\omega), \tag{A.49}$$

$$\frac{{\rm d}i}{{\rm d}\tau} = -\frac{15}{8}\frac{e^2}{\sqrt{1-e^2}}\cos(i)\sin(i)\sin(2\omega), \tag{A.50}$$

$$\frac{{\rm d}\omega}{{\rm d}\tau} = \frac{3}{4}\frac{1}{\sqrt{1-e^2}}\left\{2(1-e^2)+5\sin^2(\omega)\left[e^2-\sin^2(i)\right]\right\}, \tag{A.51}$$

$$\frac{{\rm d}\Omega}{{\rm d}\tau} = -\frac{3}{4}\frac{\cos(i)}{\sqrt{1-e^2}}[1+4e^2-5e^2\cos^2(\omega)], \tag{A.52}$$

where $$\tau \equiv \frac{2\pi}{P_{\rm orb}} \frac{M_{\rm CND}}{M_\bullet} \left(\frac{a}{R_{\rm CND}} \right)^3 t. \tag{A.53}$$

Bibliography

Alexander, R. D., Begelman, M. C., and Armitage, P. J., Constraints on the Stellar Mass Function from Stellar Dynamics at the Galactic Center, 2007, *ApJ* **654**, 907

Anantharamaiah, K. R., Pedlar, A., and Goss, W. M., 1999, Ionized Gas in the SGR A Complex – VLA Observations of H168α and H270α Recombination Lines, in H. Falcke, A. Cotera, W. J. Duschl, F. Melia, and M. J. Rieke (eds.), *The Central Parsecs of the Galaxy*, Vol. 186 of *Astronomical Society of the Pacific Conference Series*, pp 422–+

Armstrong, J. T. and Barrett, A. H., High-resolution surveys of the Sagittarius A molecular cloud complex in ammonia, carbon monoxide, and isocyanic acid, 1985, *ApJS* **57**, 535

Becklin, E. E. and Neugebauer, G., Infrared Observations of the Galactic Center, 1968, *ApJ* **151**, 145

Beloborodov, A. M., Levin, Y., Eisenhauer, F., Genzel, R., Paumard, T., Gillessen, S., and Ott, T., Clockwise Stellar Disk and the Dark Mass in the Galactic Center, 2006, *ApJ* **648**, 405

Brouwer, D. and Clemence, G. M., *Methods of celestial mechanics*, New York: Academic Press, 1961

Carruba, V., Burns, J. A., Nicholson, P. D., and Gladman, B. J., On the Inclination Distribution of the Jovian Irregular Satellites, 2002, *Icarus* **158**, 434

Christopher, M. H., Scoville, N. Z., Stolovy, S. R., and Yun, M. S., HCN and HCO^+ Observations of the Galactic Circumnuclear Disk, 2005, *ApJ* **622**, 346

Ćuk, M. and Burns, J. A., On the Secular Behavior of Irregular Satellites, 2004, *AJ* **128**, 2518

Eisenhauer, F., Genzel, R., Alexander, T., Abuter, R., Paumard, T., Ott, T., Gilbert, A., Gillessen, S., Horrobin, M., Trippe, S., Bonnet, H., Dumas, C., Hubin, N., Kaufer, A., Kissler-Patig, M., Monnet, G., Ströbele, S., Szeifert, T., Eckart, A., Schödel, R., and Zucker, S., SINFONI in the Galactic Center: Young Stars and Infrared Flares in the Central Light-Month, 2005, *ApJ* **628**, 246

Genzel, R., Crawford, M. K., Townes, C. H., and Watson, D. M., The neutral-gas disk around the galactic center, 1985, *ApJ* **297**, 766

Genzel, R., Schödel, R., Ott, T., Eisenhauer, F., Hofmann, R., Lehnert, M., Eckart, A., Alexander, T., Sternberg, A., Lenzen, R., Clénet, Y., Lacombe, F., Rouan, D., Renzini, A., and Tacconi-Garman, L. E., The Stellar Cusp around the Supermassive Black Hole in the Galactic Center, 2003, *ApJ* **594**, 812

Genzel, R. and Townes, C. H., Physical conditions, dynamics, and mass distribution in the center of the Galaxy, 1987, *ARA&A* **25**, 377

Genzel, R., Watson, D. M., Townes, C. H., Dinerstein, H. L., Hollenbach, D., Lester, D. F., Werner, M., and Storey, J. W. V., Far-infrared spectroscopy of the galactic center - Neutral and ionized gas in the central 10 parsecs of the Galaxy, 1984, *ApJ* **276**, 551

Gray, A. D., Whiteoak, J. B. Z., Cram, L. E., and Goss, W. M., Radio Continuum Observations of Sagittarius-E, 1993, *MNRAS* **264**, 678

Harris, A. I., Jaffe, D. T., Silber, M., and Genzel, R., CO 7-6 submillimeter emission from the galactic center - Warm molecular gas and the rotation curve in the central 10 parsecs, 1985, *ApJ* **294**, L93

Ho, P. T. P., Jackson, J. M., Barrett, A. H., and Armstrong, J. T., Interactions between the continuum sources in the galactic center and their immediate molecular environment, 1985, *ApJ* **288**, 575

Hyland, A. R., The galactic centre (Invited review), 1986, *Ap&SS* **118**, 343

Ivanov, P. B., Polnarev, A. G., and Saha, P., The tidal disruption rate in dense galactic cusps containing a supermassive binary black hole, 2005, *MNRAS* **358**, 1361

Jackson, J. M., Geis, N., Genzel, R., Harris, A. I., Madden, S., Poglitsch, A., Stacey, G. J., and Townes, C. H., Neutral gas in the central 2 parsecs of the Galaxy, 1993, *ApJ* **402**, 173

Kiseleva, L. G., Eggleton, P. P., and Mikkola, S., Tidal friction in triple stars, 1998, *MNRAS* **300**, 292

Kozai, Y., Secular perturbations of asteroids with high inclination and eccentricity, 1962, *AJ* **67**, 591

Landau, L. and Lifshitz, E. M., *Mechanics, Course of Theoretical Physics, Volume 1*, Pergamon Press, 1976

Lester, D. F., Werner, M. W., Storey, J. W. V., Watson, D. M., and Townes, C. H., Detection of forbidden line O I 63 micron emission from the galactic center, 1981, *ApJ* **248**, L109

Levin, Y. and Beloborodov, A. M., Stellar Disk in the Galactic Center: A Remnant of a Dense Accretion Disk?, 2003, *ApJ* **590**, L33

Lidov, M. L., The evolution of orbits of artificial satellites of planets under the action of gravitational perturbations of external bodies, 1962, *Planet. Space Sci.* **9**, 719

Lidov, M. L. and Ziglin, S. L., Non-restricted double-averaged three body problem in Hill's case, 1976, *Celestial Mechanics* **13**, 471

Mezger, P. G., Duschl, W. J., and Zylka, R., The Galactic Center: a laboratory for AGN?, 1996, *A&A Rev.* **7**, 289

Morbidelli, A., *Modern celestial mechanics : aspects of solar system dynamics*, London: Taylor & Francis, 2002, ISBN 0415279399

Paumard, T., Genzel, R., Martins, F., Nayakshin, S., Beloborodov, A. M., Levin, Y., Trippe, S., Eisenhauer, F., Ott, T., Gillessen, S., Abuter, R., Cuadra, J., Alexander, T., and Sternberg, A., The Two Young Star Disks in the Central Parsec of the Galaxy: Properties, Dynamics, and Formation, 2006, *ApJ* **643**, 1011

Press, W. H., Teukolsky, S. A., Vetterling, W. T., and Flannery, B. P., *Numerical recipes in C. The art of scientific computing*, Cambridge: University Press, —c1992, 2nd ed.

Reid, M. J., The distance to the center of the Galaxy, 1993, *ARA&A* **31**, 345

Reid, M. J. and Brunthaler, A., The Proper Motion of Sagittarius A*. II. The Mass of Sagittarius A*, 2004, *ApJ* **616**, 872

Sanders, R. H., The circumnuclear material in the Galactic Centre - A clue to the accretion process, 1998, *MNRAS* **294**, 35

Schödel, R., Eckart, A., Alexander, T., Merritt, D., Genzel, R., Sternberg, A., Meyer, L., Kul, F., Moultaka, J., Ott, T., and Straubmeier, C., The structure of the nuclear stellar cluster of the Milky Way, 2007, *A&A* **469**, 125

Schödel, R., Ott, T., Genzel, R., Eckart, A., Mouawad, N., and Alexander, T., Stellar Dynamics in the Central Arcsecond of Our Galaxy, 2003, *ApJ* **596**, 1015

Shapley, H., Studies based on the colors and magnitudes in stellar clusters. VII. The distances, distribution in space, and dimensions of 69 globular clusters., 1918, *ApJ* **48**, 154

Shukla, H., Yun, M. S., and Scoville, N. Z., Dense, Ionized, and Neutral Gas Surrounding Sagittarius A*, 2004, *ApJ* **616**, 231

Vollmer, B. and Duschl, W. J., A cloudy model for the Circumnuclear Disk in the Galactic Centre, 2001, *A&A* **367**, 72

Yusef-Zadeh, F., Lasenby, A., and Marshall, J., Highly blueshifted H I gas toward the Galactic center, 1993, *ApJ* **410**, L27

Yusef-Zadeh, F., Melia, F., and Wardle, M., The Galactic Center: An Interacting System of Unusual Sources, 2000, *Science* **287**, 85

Zhao, J.-H., Goss, W. M., and Ho, P. T. P., VLA OH Observations of High Negative Velocity Gas toward Sagittarius A West: A High-Velocity Cloud Interacting with the Galactic Center, 1995, *ApJ* **450**, 122